2014

# Solid state NMR studies of the location, immobilization and conformation of short chain branches in semicrystalline polyethylene-hexene copolymers

Allison L. White
*Iowa State University*

# Solid state NMR studies of the location, immobilization and conformation of short chain branches in semicrystalline polyethylene-hexene copolymers

by

**Allison L. White**

A thesis submitted to the graduate faculty

in partial fulfillment of the requirements for the degree of

MASTER OF SCIENCE

Major: Chemistry

Program of Study Committee:
Patricia Thiel, Major Professor
Klaus Schmidt-Rohr
Gordon Miller
Theresa Windus

Iowa State University

Ames, Iowa

2014

TABLE OF CONTENTS

Page

# ACKNOWLEDGEMENTS

Thanks to my research mentor for this work, Klaus Schmidt-Rohr, for the hours you spent with me at the spectrometer and for your example of always working until the experiment, the analysis, or the figure is just right – even during and after moving a lab.

Thanks to my major professor (again), Pat Thiel, for your continuing encouragement and the opportunity to build my teaching experience in CHEM 325. Thanks to my other committee members, Gordie Miller and Theresa Windus, for your guidance and support through every iteration of my Program of Study.

Thanks to my friends, fellow students and group members: some for willingness to listen and share their own experiences, some for time spent training me, some for working together to tackle Fundamentals of Quantum Mechanics, and some for swapping cat stories. All of you have helped me to persevere through the twists and turns of my career so far at ISU.

Thanks to my husband, Lucas, my partner through this and much more.

# ABSTRACT

Distinct localization of butyl branches in high- and linear low-density polyethylenes (HDPEs and LLDPEs) has been detected by solid-state $^{13}C$ NMR (ssNMR). Several important mechanical properties of polyethylene materials, such as their deformation in response to stress, depend on the composition and connectivity of the noncrystalline interlamellar phase. Even with spectral editing, the $^{13}C$ NMR signals from segments in the crystalline-noncrystalline interfacial region, or generally with intermediate mobility, usually overlap with signals from either the noncrystalline or the crystalline segments. We have introduced double inverse filtering as a systematic, robust approach to selectively observe the signals from these intermediate-mobility segments.

This approach is applied to a set of HDPE and LLDPE copolymers with 0.35-3.3 mol% hexene. Two branch types are delineated: (i) mobile amorphous branches with faster $^{13}C$ spin lattice relaxation and more motional averaging of NMR interactions, and (ii) trans-rich limited-mobility branches with slower $^{13}C$ spin lattice relaxation and less motional averaging. Using $^{1}H$ spin-diffusion experiments and $T_{1\rho H}$ measurements, it is also shown that the limited-mobility butyl branches accumulate near the crystalline-noncrystalline interface. Their number is shown to remain approximately constant at about 0.5 mol% for the range of hexene content covered by this study. This roughly matches one branch immobilized at every point where a chain emanates from the crystal; for an HDPE with less than 0.5 mol% hexene, nearly all branches are found at the crystal surface.

# CHAPTER 1: GENERAL INTRODUCTION

## Project Background and Scope

The polyethylene class of macromolecules contributes two of the six polymers that dominate the polymers industry: HDPE (high-density polyethylene) and LLDPE (linear low-density polyethylene).[1] Polyethylene structure was made much easier to control with the adoption of metallocene catalysts in the early 2000s.[2] More recently, polyethylene production has been one beneficiary of lowered natural gas prices due to the tapping of shale formations.[3] This is because the monomers – ethylene and other related molecules (called alpha-olefins) – can be produced from the ethane extracted from natural gas. The LLDPE type of polyethylene is composed of ethylene subunits mixed with longer alpha-olefins that create short branches off of the main backbone produced by the ethylene. The branches get in the way when the polymer solidifies and inhibit the packing of the polymer into its compact crystal form. More of the polymer ends up in a noncrystalline form that takes up more space, making the bulk material less dense (hence the name) and more pliable. The HDPE type may have short branches as well, but fewer than an LLDPE has. As a result, more of each HDPE molecule is able to pack into the crystal form and bulk HDPE is denser and more rigid than LLDPE.

In both HDPE and LLDPE, the areas of tightly packed crystalline polymer (crystallites) are separated by noncrystalline regions where the polymer is less organized, less dense, and able to move more freely. In some polyethylenes with methyl or ethyl branches, the branches are able to fit into the crystallites. However,

in the samples studied here, the branches are too long, so all of the branches must remain in the noncrystalline region. Between the crystallites and the noncrystalline region is a boundary layer (the interfacial region or interphase) where the polymer molecules exit or enter the crystal. Some of the molecules stretch across the noncrystalline region to the next crystallite, some come to an end in the noncrystalline region, and some loop back around to re-enter the same crystallite.

Materials with a range of short branch contents, chain lengths, and levels of crystallinity were prepared by our colleagues at Exxon Mobile Research and Engineering Company (EMRE). I used a suite of solid-state NMR (ssNMR) experiments combining different techniques to initiate and manipulate the magnetic polarization of the carbon-13 ($^{13}C$) nuclei and hydrogen ($^{1}H$) nuclei located in selected types of polymer segments. These manipulations enabled us to distinguish segments within the crystal from those in the noncrystalline regions or at the crystalline-noncrystalline interface. We were also able to distinguish segments with fast and slow motions, large- and small-amplitude motions, or straight or twisted conformations from each other.

This study was intended to address several open questions about branched polyethylene, and more specifically about a set of ethylene-hexene copolymers with densities in the LLDPE or HDPE range:

1. What are the properties of the parts of the polymer molecules that are located in the interfacial region? How do they move, and how are they positioned?

2. What fraction of the polymer material is located in interfacial regions, instead of clearly within the crystallites or the noncrystalline regions?
3. Where are the branches located in the noncrystalline region: do they accumulate in the area farthest from the crystallites, do they stay close to the interface, are they spread evenly throughout?

## Thesis Organization

In Chapter 2, I describe polyethylenes in general and the samples chosen for this study in more detail. In Chapter 3, I give some background about the underlying principles of the NMR experiments. In Chapter 4, I give the details of the specific NMR experiments that were applied to the above questions and describe how the samples were prepared for NMR analysis. In Chapter 5, I present excerpts from a paper describing the identification and characterization of limited-mobility butyl branches located in the interfacial region of the ethylene-hexene copolymers.

# CHAPTER 2: POLYETHYLENE BACKGROUND

## About the Material

Polyethylenes are widely used materials that are relatively inexpensive and are produced in very large quantities for an enormous number of applications.[1, 3] The crystallites in most industrially-produced PEs have the orthorhombic crystal structure shown below with the chains oriented in a "herringbone" pattern relative to their neighbors and a density of 1.00 g/cm$^3$ (Fig. 2.1).[4] Polyethylene (PE) molecules can form other crystalline structures, but this is by far the most commonly encountered structure under normal synthetic conditions for industrially-produced materials.[2,4]

Except in specially prepared single-crystal samples, solid PE materials are not totally crystalline. They are semicrystalline polymers; crystalline regions (crystallites) do exist but they are separated from each other by more disordered regions. On a scale of about 10 nm, those noncrystalline regions are sandwiched between crystallites in a layered (lamellar) structure. This alternating pattern does not extend indefinitely; a stack of layers (lamellae) can be oriented to nearby stacks of lamellae in different ways to produce larger structures like spherulites or "shish kebabs".[4] The length of a single PE molecule is often significantly greater than the thickness of the lamellae in the "c" direction, so individual molecules may pass through multiple crystallites. The phase structure is detailed further later in this chapter.

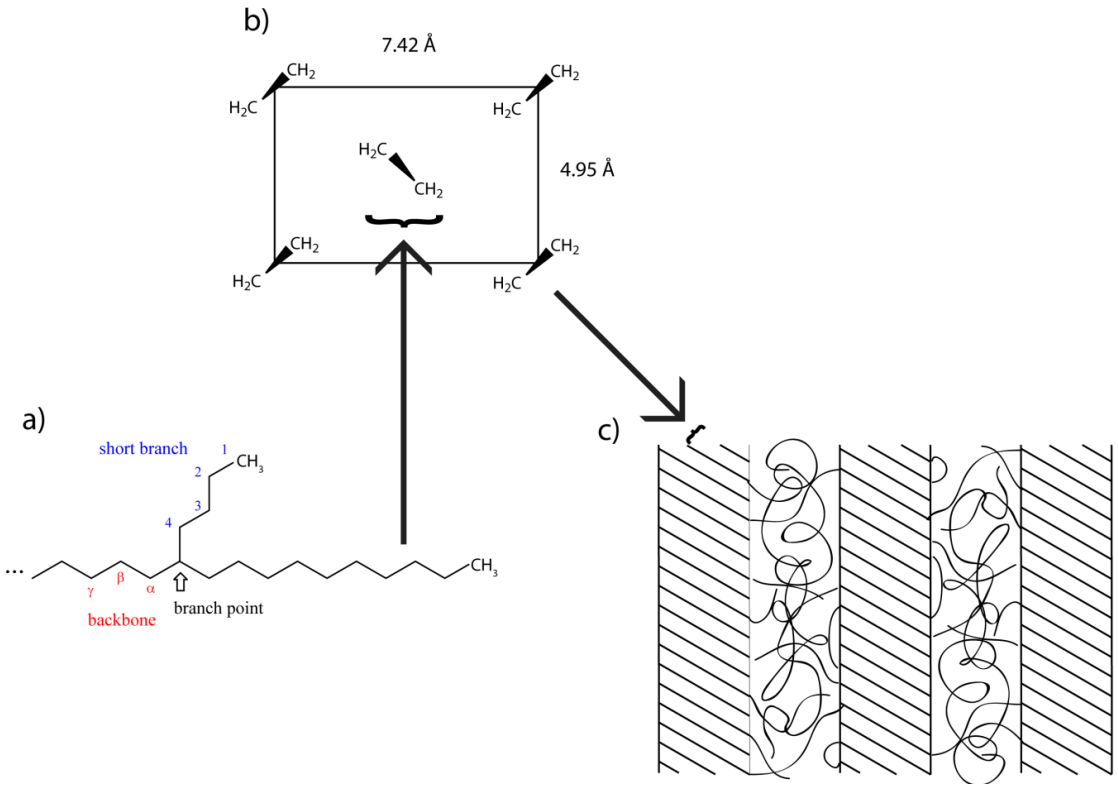


**Figure 2.1.** Illustration of polyethylene structure and morphology on multiple scales: a) portion of a single PE molecule with short branch and chain end shown; b) view (down the length of the chains) of crystalline PE unit cell[4, 5]; c) illustration of lamellar arrangement of crystallites and noncrystalline regions; scale is representative only where distances are indicated, chain positions and conformations in the amorphous regions are stylized

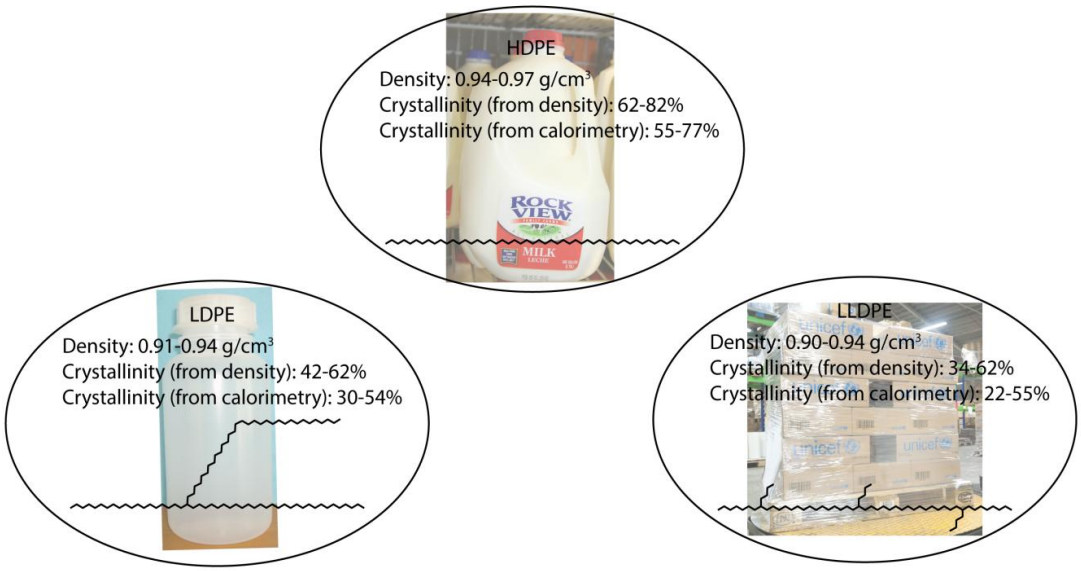


**Figure 2.2.**Differences in properties and applications between three major forms of polyethylene[4]

## Forms of Polyethylene

Polyethylenes can be produced in ways that give a range of mechanical properties. They are used primarily for packaging and storage. The three most-used classes of polyethylenes are high-density (HDPE), low-density (LDPE), and linear low-density (LLDPE). Each class in turn includes many different materials, but these broad categories are useful in situations such as sorting plastic products for recycling.

HDPEs are used in consumer products such as milk jugs and shampoo bottles and are designated by the recycling number 2. Their long backbone chains branch very little and they possess high crystallinity and therefore high density and rigidity. An HDPE may include some short-chain branches while maintaining sufficiently high density to retain that classification. LDPEs are used when more flexibility is required, as in squeeze bottles for laboratory reagents or in trash bags. The density difference between LDPEs and HDPEs is attributed to the backbone branching in LDPEs that interrupts the formation of crystallites. LLDPEs are used in the tough films required for packaging products like produce. The low crystallinity and density of LLDPEs are consequences of short-chain branches introduced by other alpha-olefin monomers (e.g., propene, butene, hexene), instead of by the long-chain branches that cause the lower density of LDPEs.

The materials studied in this project are ethylene-hexene copolymers with properties that fall within the ranges associated with LLDPE and HDPE. Although all of the materials contain an additional alpha-olefin monomer (hexene) and would normally be considered LLDPEs, some have high enough densities that they fall

within the HDPE classification, as can be seen in the characterization data provided by Dr. K. Mao. (Table 2.1)

Characterization and Physical Properties

**Density Measurements**

Density is closely related to crystallinity (the fraction of the material that contributes to crystallites), since the regions of crystalline-packed polyethylene are denser than the interface and noncrystalline regions. All other things held equal, a more-crystalline polyethylene sample will be denser than a less-crystalline sample. Density measurements can therefore be used to calculate the crystallinity of a sample.[6] A positive correlation between density and crystallinity (as measured by NMR) can be seen in Table 2.1.

**Molecular Weight**

The average molecular weight of a polymer can be quantified in multiple ways. The number average of the molecular weight of each chain ($M_n$) is the most relevant to our discussion later, but other averages are also useful to describe the spread and skew of the distribution of chain lengths that exist in a given material.[4, 7] The $M_n$ values of the samples used in this study correspond to 780-4700 methylene ($CH_2$) units per molecule. (Table 2.1)

**Table 2.1.** Summary of previous characterization of ethylene-hexene copolymer samples, from unpublished data provided by K. Mao. Hexene amount is the mole percent of hexene, as opposed to ethylene, in the polymer product. Molecular weight is provided as the number average ($M_n$). The long period ($L_p$) in the lamellar stacks and the thickness ($L_c$) of the crystalline lamellae are reported from small-angle X-ray scattering (SAXS). The fractions of each sample in the crystalline, intermediate, and amorphous phases ($x_c$, $x_i$, and $x_a$, respectively) are reported from solid-state NMR (ssNMR).

| sample | hexene (mol%) | density (g/cc) | molecular weight ($M_n$ , kg/mol) | SAXS | | ssNMR | | |
|---|---|---|---|---|---|---|---|---|
| | | | | $L_p$ | $L_c$ | $x_c$ | $x_i$ | $x_a$ |
| **PE-h0.35** | 0.35 | .95 | 42 | 32.7 | 18.5 | 51.8 | 10.2 | 38 |
| **PE-h0.9L** | 0.9 | .95 | 20 | 24.1 | 13.4 | 42.9 | 11.7 | 45.4 |
| **PE-h0.9H** | 0.9 | 0.934 | 52 | 25.5 | 11.2 | 31 | 12.3 | 56.6 |
| **PE-h1.2** | 1.2 | 0.935 | 37 | 24.1 | 10.9 | 31.9 | 12.2 | 55.9 |
| **PE-h2.0** | 2.0 | 0.919 | 66 | 22.1 | 8.0 | 24.7 | 13.8 | 61.5 |
| **PE-h2.3** | 2.3 | 0.919 | 54 | 20.5 | 7.2 | 25 | 14 | 60.9 |
| **PE-h2.8** | 2.8 | 0.92 | 41 | 20.8 | 7.1 | 24.1 | 14.4 | 61.4 |
| **PE-h3.3** | 3.3 | 0.92 | 25 | 18.2 | 6.8 | 26.6 | 15.9 | 57.4 |
| **PE-h4.4** | 4.4 | 0.92 | 11 | 22.3 | 8.4 | 27.3 | 16.7 | 55.9 |

## X-Ray Scattering Methods

The wide-angle x-ray scattering (WAXS) of semicrystalline polyethylene is used to estimate both the dimensions of the crystallites along several crystallographic directions and the crystallinity of the material.[6, 8] Small-angle x-ray scattering (SAXS) can provide the length of one lamellar repeat (one crystallite and one noncrystalline layer) and the length of the crystallites along the direction perpendicular to the lamellae.[6, 9]

## Calorimetry

Differential scanning calorimetry (DSC) is a method in which a sample is heated in a controlled manner and the enthalpy change is monitored. At the melting or crystallization temperature, the DSC trace shows peaks whose area is the heat of fusion. The melting temperature depends on the crystal thickness and the heat of fusion depends on the degree of crystallinity.

**Solution and ssNMR[10-16]**

Solution and solid-state NMR methods have been used to quantify aspects of polyethylene composition since the 1950's[17-19], and the power and versatility of those methods have increased as the field as a whole has grown. Solution NMR methods are used in studies of PE melts, while ssNMR is used on the crystallized PE products. Direct-polarization ssNMR with a selection of recycle delays[20] yields the fractions of semicrystalline polyethylene within the crystallites, within the noncrystalline regions, and within the interface. This is the method used to obtain the values listed in Table 2.1.

These NMR methods for PE analysis are based on the collection of quantitative $^{13}C$ NMR spectra – spectra that include fully representative signals from every $^{13}C$ species present in the sample – and integration of the peak areas assigned to particular $^{13}C$ species. In order to collect a quantitative spectrum, recycle delays between individual scans must be on the order of 1000 s in order to accommodate the slow return of the crystal magnetization to its equilibrium value after each repetition (scan) of the experiment. This makes collecting fully quantitative spectra undesirable from the perspective of time efficiency, and it is helpful to design shorter experiments that are informative without being fully quantitative in that way. Other reasons that a spectrum that only contains signal from some $^{13}C$ species might be desirable, aside from time efficiency, are addressed in Chapter 3.

## Structural Model

Since individual polyethylene chains are typically longer than the width of the crystallites or noncrystalline regions, they can and do extend between multiple crystallites. The middle sections of the molecules that cross a noncrystalline region, while forming part of a crystallite on either side, are called tie molecules. The ends of molecules located in the noncrystalline region are called cilia. Many molecules have a middle section in a noncrystalline region and both ends in the same crystallite (chain re-entry). The presence, frequency, and orientation of reentering molecules, tie molecules, and cilia form a significant part of the issues investigated by PE research, especially that focusing on deformation of PE materials. [21-28] A model for the connectivity at the interface is necessary for interpreting measurements of the relative proportions of different phases and of the degree of crystallinity. Having an accurate model of connectivity is also important because the amounts and properties of molecules crossing the crystalline/noncrystalline interface, tie molecules in particular, have consequences for important mechanical properties such as stress response and stiffness.[4]

While the most common model of the phase structure of lamellar polyethylene only includes two phases – crystalline and noncrystalline – spectroscopic and diffraction studies have provided evidence for a third interfacial phase, sometimes called the interphase, that physically separates them. [8, 9, 29] Instead of thinking of the interface as a discrete boundary, it is more appropriate to consider an interfacial region when examining the properties of the molecules which cross the interface, and to anticipate gradients of properties instead of abrupt

changes. The data underpinning models of PE phase structure have come in large part from NMR investigations.[10, 11] The capabilities of quantitative and selective NMR experiments to yield information about backbone and branch mobility, conformation, and location within the lamellar environment make them an integral part of the ongoing research effort to describe and model the phase structure of PEs.

# CHAPTER 3: NUCLEAR MAGNETIC RESONANCE BACKGROUND

## Principles

### Experiment Basics[30, 31]

The nuclear magnetic resonance (NMR) experiment begins with the application of a controlled duration of radiofrequency radiation (pulse) by an induction coil surrounding the sample. The magnetic field created by the main magnet (the external field, $B_0$) is much greater in magnitude than the magnetic field created by the coil (the pulses, $B_1$). The external field is large because it is desirable in NMR to create a larger population difference between the spin state that is aligned with the field and the spin state aligned against the field. The larger the population difference, the larger the electronic signal that is eventually recorded and converted into the spectrum. The strength of the external field is often reported in terms of a frequency $\omega_0$:

$$\omega_0 = -\gamma B_0 \quad (1)$$

where $\gamma$ is the gyromagnetic ratio of the nucleus (usually $^1H$) being used to describe the field strength of the magnet. The "400 MHz" spectrometer used in this study includes a magnet with a $B_0$ field of 9.4 T.

The raw dataset produced by the experiment is the free induction decay (FID) curve created by the oscillation of the component of the magnetization that lies in the xy plane relative to $B_0$, which defines the z-direction in the lab frame of reference. The FID curve is Fourier transformed to give a spectrum in the frequency domain, instead of a decay curve in the time domain. Mathematical treatments of the

data such as Gaussian broadening may be used to reduce the effect of noise on the spectrum at the expense of resolution. The x-axis of the spectrum may be labeled in frequency units, but is more often seen with units of ppm (indicating the fractional difference of the observed frequency from a reference frequency).

**Polarization**

The spin polarization of the nuclei in an NMR sample can be described as the difference in population between the "up" and "down" spin states, which are aligned with and against the $B_0$ field, respectively. The spin polarization can be manipulated by the application of radiofrequency pulses. The experiments employed in this study either begin with a single-pulse excitation (direct polarization, DP) of the nucleus ($^1H$ or $^{13}C$) to be observed or with excitation of $^1H$ nuclei followed by transfer of magnetization (cross polarization, CP) to $^{13}C$ nuclei via another kind of pulse. The reasons for using each type of polarization method are explained in Chapter 4.

**Spin Evolution and Relaxation**

Pulse intensities and lengths are tuned to cause specific oscillations (better called precessions or nutations, since they occur in more than one dimension) in the orientation of the net magnetic polarization of the nuclear spins. A $\pi/2$ pulse is of the power and duration necessary to rotate the orientation of the net polarization through 90 degrees, a $\pi$ pulse to rotate through 180°, a CP transfer pulse to cause buildup of the $^{13}C$ magnetization at the expense of the $^1H$ magnetization, and so on. The strength of the pulses can be expressed as the frequency of the nutation that they will induce in the net polarization of the nuclear spins. Pulse strength can be

described in terms of the magnitude of the magnetic field $B_1$ or the induced frequency $\omega_1$ as seen above:

$$\omega_1 = -\gamma B_1 \quad (2)$$

A pulse perturbs the system of nuclear spins, and after the pulse ends the net magnitude and direction of the polarization will change until they return to their equilibrium values, with the net polarization oriented along the z-axis defined by $B_0$ and a magnitude that reflects the equilibrium populations of the spin-up and spin-down states. The process of returning to equilibrium is called relaxation, and several forms of relaxation (and their associated rates) are employed in this study to distinguish the signals of different types of $^1H$ and $^{13}C$ nuclei.

The time constant associated with longitudinal relaxation is called $T_1$. As longitudinal relaxation progresses the net magnetization in the z-direction changes until it reaches its equilibrium magnitude. $T_1$ has a minimum for motions producing fluctuating magnetic fields with rates near the Larmor frequency $\omega_0$. The time constant associated with longitudinal relaxation under the spin-lock conditions imposed during cross-polarization is called $T_{1\rho}$.

The time constant associated with transverse relaxation is called $T_2$ . As transverse relaxation progresses the net magnetization in the xy plane decreases asymptotically towards zero. A similar effect arises when the nutation frequency of all nuclei is not exactly equal, and as time goes on the differences in frequency lead to a “fanning out” of what originally could be represented as a single vector. This produces a reduction of the net polarization in the xy plane with a time constant $T_2^*$.

The signal decrease due to $T_2^*$ can be refocused by a spin echo; the signal decrease due to $T_2$ generally cannot be refocused in that way.

These time constants are related to the associated exponential decay or exponential buildup of magnetization by the exponential relation below:

$$M(t) = M_0 e^{-t/\tau} \; ; \; \tau = T_1, T_2, \text{etc.} \tag{3}$$

In Equation 3, M(t) is the magnetization at a certain time t, and $M_0$ is the magnetization at t=0. Correlation times may be written with an additional subscript indicating the nucleus to which they refer (e.g., $T_{1C,}$ $T_{1s\rho H}$).

Local Fields and Other Effects

**Dipolar Coupling and Dephasing[31]**

Since we do not study atomic nuclei in a vacuum, the effect of nearby nuclei and electrons must be considered. One effect that neighboring nuclear magnets have on the evolution of the magnetization is mediated by the dipolar field. The dipolar field is dependent on orientation in the sense that its magnitude depends on the cosine squared of the angle between the internuclear vector and the external field $B_0$[31]. The strength of the magnetic field experienced by a nucleus due to nearby dipoles can be expressed as a frequency, just as $B_0$ and $B_1$ above. That frequency depends on the z-component of the dipolar field:

$$\omega_{dip} = -\gamma B_{dip,z} \tag{4}$$

The strength of the dipolar coupling can also be expressed as the characteristic time of the exponential decay (or "dephasing") of the magnetization due to the dipolar field. This characteristic time can be written like $T_{CH}$, indicating the pair of nuclei under consideration, and is defined in the same way as the

relaxation times discussed above. The magnetization of nuclei which are strongly affected by the dipolar field created by their neighbors will be dephased faster (will have a shorter $T_{CH}$).

Many of the experiments described in Chapter 4 include "$^{1}$H decoupling" for parts of the experiment. During those periods of time, the $^{1}$H nuclei are being irradiated in such a way that the $^{13}$C nuclei will not be affected by their dipolar field and will not experience dipolar dephasing.

**Chemical Shift Anisotropy[31]**

The chemical shift, perhaps the most familiar NMR observable, does not have a single fixed value for a nucleus in a particular chemical environment. The magnitude of the chemical shift is anisotropic – its value varies depending on the direction of the magnetic field relative to the segment containing the nucleus. The anisotropy in the chemical shift can be defined by the parameters δ and η or by certain values in the 3-by-3 matrix, or tensor, that describes the values of the chemical shift in all directions. The total chemical shift can be split into isotropic (orientation-independent) and anisotropic (orientation-dependents) parts:

$$\omega_{CS} = \omega_{iso} + \omega_{CSA} \quad (5)$$

The frequency associated with the CSA depends on the angle θ formed between the principal axis of the chemical shift tensor and the external magnetic field (in general, different from the corresponding angle important in dipolar coupling) according to the following equation:

$$\omega_{CSA} = \frac{\delta}{2}(3\cos^2\theta - 1 - \eta\sin^2\theta\cos 2\phi) \quad (6)$$

**Magic Angle Spinning[32]**

In a solution- or liquid-state experiment, the tumbling of the molecules causes each observed chemical shift to be an average, making it appear to have a single value. In solids, isotropic tumbling motions are usually not fast enough to cause this averaging, and in static (non-spinning) experiments, broad lines are observed, with characteristic shapes described by the parameters mentioned above.

When the CSA parameter η=0, the equation for the dependence of frequency on θ simplifies to:

$$\omega(\theta) = \frac{\delta}{2}(3\cos^2\theta - 1) \qquad (7)$$

When the sample is rapidly rotated around an axis at an angle of 54.74° to $B_0$, anisotropic contributions to the chemical shift frequency ($\omega_{CSA}$) are refocused and $\omega_{CS} = \omega_{iso}$ at the end of full rotation periods. NMR experiments performed while a sample is spinning under these conditions are called magic-angle spinning (MAS) experiments. In this way, the effect of the tumbling in a liquid sample can be artificially replicated and the spectra recorded in MAS experiments reflect only the isotropic chemical shift of each nucleus.

**The Gamma-Gauche Effect**

The gamma-gauche effect is the change in the isotropic chemical shift of a particular $^{13}C$ species in alkanes, including polyethylenes, based on the relative position of its neighbors in the backbone, as illustrated in Figure 3.1.[16] A $^{13}C$ species that has only trans C-C bonds on each side has a certain characteristic chemical shift (e.g., 33 ppm for PE). If the same $^{13}C$ species has only gauche C-C bonds on each side, its chemical shift will be lower than the all-trans position by about 8 ppm, and if it

has gauche C-C bonds on one side and trans bonds on the other, its chemical shift will be lower than the all-trans position by about 4 ppm. If 25% of the $^{13}C$ nuclei of that type were stuck in an all-gauche conformation and 75% were stuck in an all-trans conformation (or conversion between the conformations was sufficiently slow), two peaks would be expected: one at the all-trans chemical shift and one at the all-gauche chemical shift, with the all-trans peak three times as intense as the all-gauche peak.

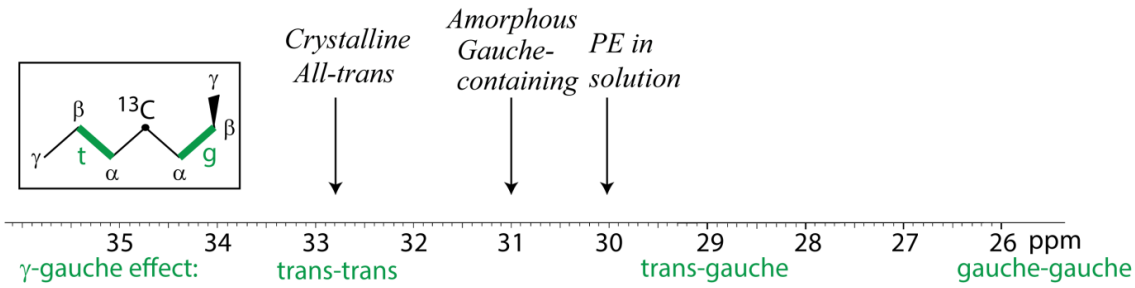


**Figure 3.1.** Illustration of the gamma-gauche effect on $^{13}C$ chemical shifts in polyethylene

Since the rate of exchange between conformations in the noncrystalline regions of PE is fast on the time scale of the NMR experiment (~ 1 ms), the observed peak for a species reflects the average conformational environment in which that species is found. For example: if 25% of the C-C bonds associated with a particular noncrystalline species are trans and 75% are gauche, the fast conversion between trans and gauche will create an observed peak that is a weighted average of the chemical shifts. Such a peak would be expected to appear at about 2 ppm lower chemical shift than the all-trans conformation.

# CHAPTER 4: EXPERIMENTAL METHODS AND PRELIMINARY WORK

## Sample Preparation

Samples for this study were synthesized and provided by ExxonMobil Research and Engineering Company (EMRE). The materials were provided by EMRE as dog-bone shaped pieces approx. 32 mm by 26 mm by 3.5 mm. We decided to change the standard procedure described by our collaborators for loading rotors with the polymer sample. By maximizing the filling factor (the percent of the coil volume which is filled by the sample), we could improve the signal obtained with each scan. Instead of cutting the dog-bone into many small chunks and filling the rotor with those chunks, which would leave a significant amount of empty space, we cut out circular pieces of the dog-bone so that the pieces could be stacked into a cylinder matching the interior dimensions of the rotor. We used an arbor press and a punch to cut out disks of the necessary diameter.

The inner diameter of the punch blade did not exactly equal the diameter of the resulting disk due to expansion when the disk is removed from the punch, so it was necessary to test and adjust the punch diameter to get the desired disk size. The cutting edge of the punch determined the shape of the resulting disk as well. If the blade wasn't sharp, the sides of the disk would slant toward each other, creating a trapezoidal profile. If the blade wasn't kept round, the disk would be oblong. If the disk was punched out too close to an existing hole or the edge of the sample, the sides of the disk would be slanted to one side, creating a parallelogram profile.

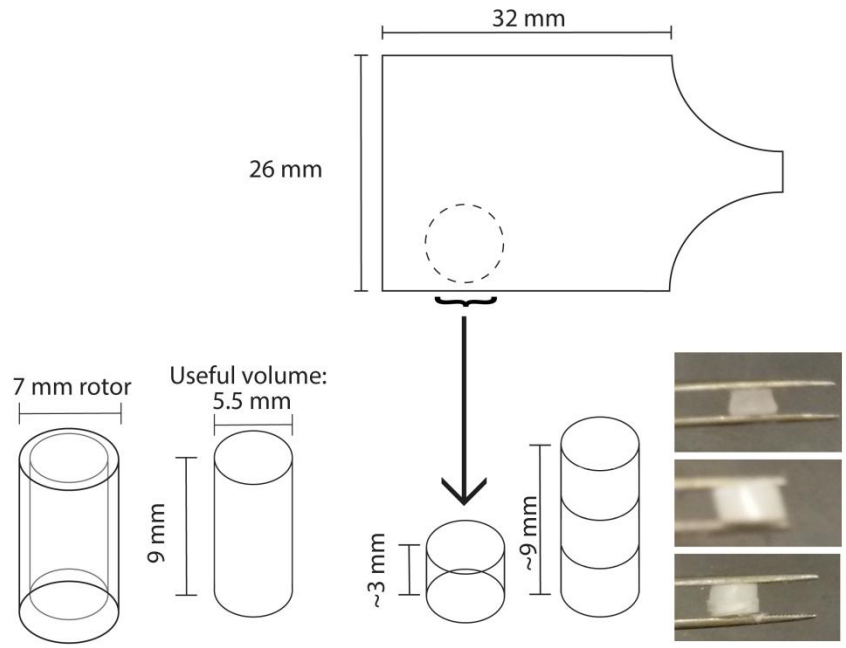


**Figure 4.1**. Preparation of a PE dog-bone sample for loading into an ssNMR rotor

For these reasons, it was helpful to sharpen and round the punch after about every three uses to avoid wasting material on incorrectly shaped disks. It was also important to use a backing material that would keep the sample from bending as pressure was applied. Of a wooden block, a rubber sheet, and a Teflon sheet, the Teflon sheet provided the best backing material. If the disks in a particular rotor tended to slide up and down despite meeting the diameter specifications, a single layer of Teflon tape was used to wrap the stack of disks. This extra layer added the necessary width and friction to hold the disks in place, and enabled easier removal of the stack of disks if the rotor needed to be unpacked.

## NMR Experiments

### Instrumentation and Software

The solid-state magic angle spinning NMR studies were carried out on a Bruker 400 MHz spectrometer at a $^{13}C$ frequency of 100 MHz. A 7-mm MAS

probehead was used for maximum signal, with 4 kHz magic angle spinning and high-power $^{1}H$ decoupling. Experiments were run using Bruker XWinNMR version 3.5. Peak areas and other measurements were evaluated using Bruker XWinNMR 3.5 or TopSpin 3.2.

**Spectral Editing: Regular and Inverse Filtering**

In most of the methods described below, the pulse sequences were modified from their most basic form to manipulate the relative intensity of the signals associated with certain $^{13}C$ or $^{1}H$ nuclei. This strategy is known as spectral editing or filtering. The pulse sequence modifications (filters) are designed to take advantage of differences in relaxation, diffusion, or dephasing rates in order to suppress or enhance some signals relative to others.[12] In some cases, the filtered spectra resulting from these experiments were sufficient for our purposes; in other cases, we needed to examine the signals that had been filtered out. To do this, two spectra were measured: one with a basic unfiltered experiment, and one with a filtered experiment. The area of the filtered spectrum was then subtracted from the area of the unfiltered spectrum to produce an inverse-filtered spectrum that, although not directly measured, can provide valuable information. The inverse-filtered spectrum shows the intensity and types of signals that were removed by the filter in the measured spectrum. Regular spectral editing and inverse filtering both play important roles in the following experiments.

**Experiments Using $^{1}H$-Detection**

Single-pulse $^{1}H$ experiments with $T_{2,H}$ regular and inverse filtering were used to evaluate the relative amounts of very rigid (crystalline), very mobile

(amorphous) and intermediate-mobility components in each sample.[33] A preliminary investigation of the $T_{2H}$- and inverse $T_{2H}$-filtered spectra of an HDPE sample and an LLDPE sample (Fig. 4.2) demonstrated the existence of a significant contribution (only in the LLDPE) from polymer segments that are more rigid than the normal noncrystalline segments, but more mobile than the crystalline segments.

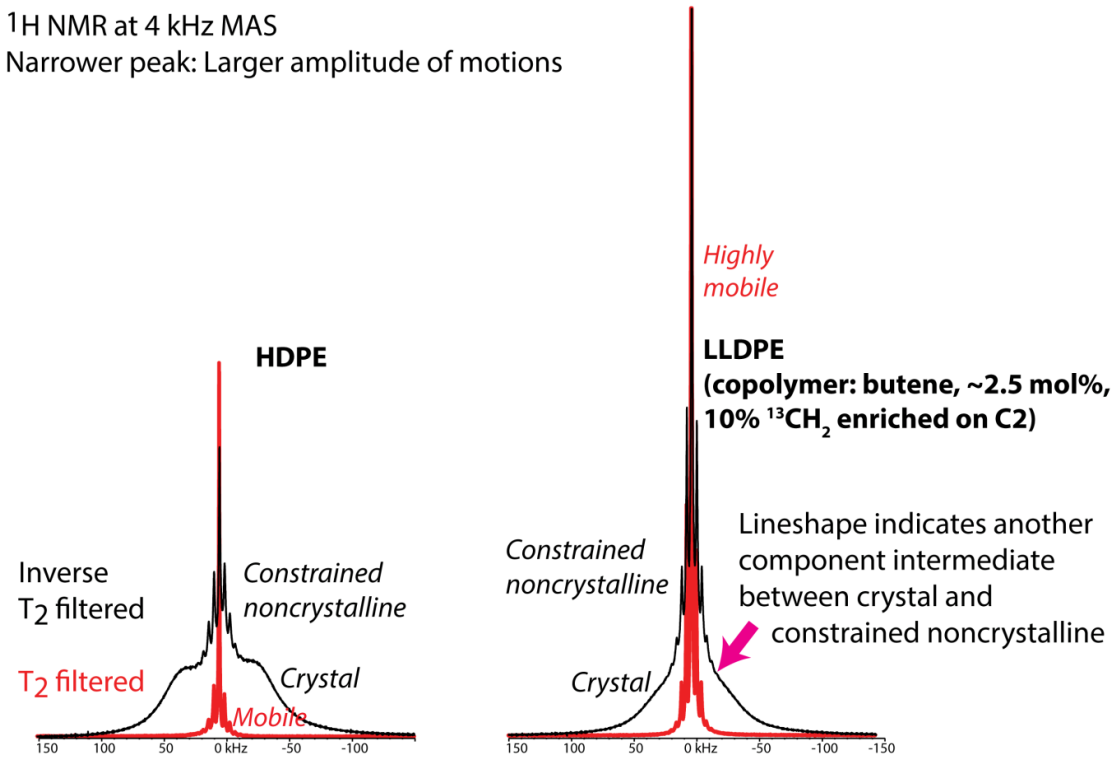


**Figure 4.2**. Preliminary spectra from $^{1}H$ single-pulse experiments on HDPE and LLDPE

**Experiments Using $^{13}C$-Detection**

Direct Polarization

Direct-polarization (DP) experiments were used to obtain spectra in which the least-mobile component, the crystal, is suppressed due to the very long $T_{1C}$ of that component and the selection of a relatively short recycle delay. The recycle delay in a DP experiment acts as a filter during which the longitudinal magnetization

of the crystalline $^{13}C$ nuclei cannot fully relax. A basic pulse diagram for a DP experiment is shown in Fig. 4.3a.

Gated decoupling, a type of dipolar dephasing filter, was applied to the DP experiments to suppress the signal from components containing $^{13}C$ nuclei with stronger $^{13}C$-$^{1}H$ heteronuclear dipolar coupling (short $T_{CH}$) due to the lower mobility of those segments.[31] The pulse diagram in Fig. 4.3b illustrates the timing of the dipolar dephasing period in a DP experiment. The filtered spectra show signals from highly mobile noncrystalline components with short $T_{1C}$ and long $T_{CH}$, while the corresponding inverse-filtered spectra show signals from rigid noncrystalline components with short $T_{1C}$ and long $T_{CH}$.

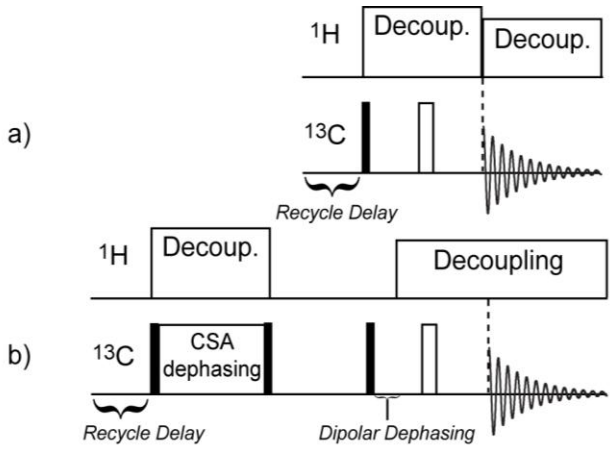


**Figure 4.3.** a) Basic DP pulse sequence with Hahn echo; b) sample DP pulse sequence for a more complex experiment: CSA dephasing with double inverse filter

CP – Experiments Using $^{1}H$ Magnetization Transferred to $^{13}C$ for Detection[14, 16]

In a similar way, cross-polarization (CP) experiments were conducted to measure spectra associated with $^{1}H$-based observables. The basic CP experiment is shown in Fig. 4.4a. The basic set of filters described above ($T_{1C}$ relaxation and C-H dipolar dephasing) was augmented with $T_{1\rho}$ filters or Goldman-Shen spin-diffusion periods to probe the relative locations of components, or CSA dephasing periods to

compare the rate of motion of components. The timing of these additional components is illustrated in Fig. 4.4b-c.

The intensity of signal associated with long-$T_1$ $^{13}C$ species does not depend on the recycle delay of CP experiments in the same way that it does in DP experiments because of the polarization transfer from $^{1}H$ to $^{13}C$ during the pulse sequence. Since the CP recycle delay cannot be used as a $T_{1C}$ filter, a $T_{1C}$ relaxation period was included in the CP experiments between the polarization transfer and data acquisition. A gated decoupling period for dipolar dephasing was included in the pulse sequence in the same way as in the DP experiments. By collecting spectra with different combinations of $T_{1C}$ and dipolar dephasing filters, we can prepare a double inverse filtered spectrum based on CP experiments. See Figure 5.1 for a summary of DP- and CP-based double inverse filtering using one ethylene-hexene copolymer as an example.

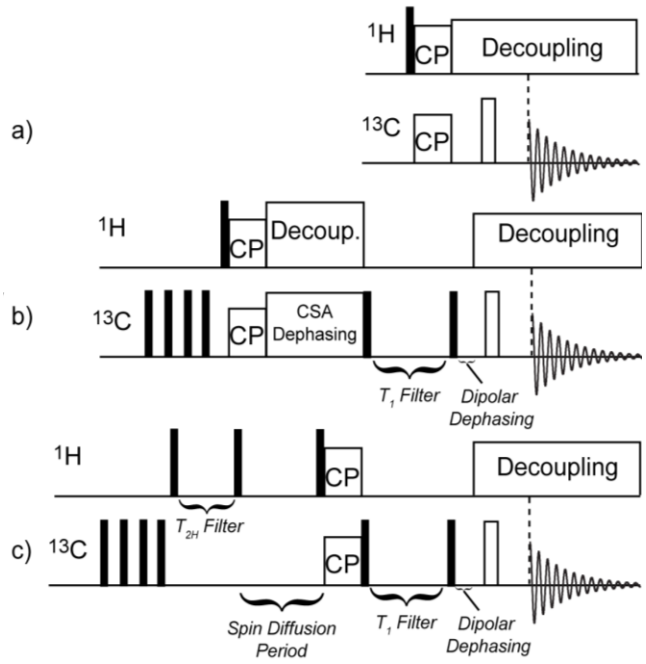


**Figure 4.4.** a) Basic CP pulse diagram with Hahn echo; b), c) sample CP pulse sequences for more complex experiments: b) CSA dephasing with double inverse filter, c) spin diffusion with double inverse filter

WISE

The basic set of filters was also applied to the WISE (two-dimensional WIdeline SEparation NMR spectroscopy) experiment to correlate the $^{1}H$ spectra and their associated mobility information to the various components separated by filters on the $^{13}C$ dimension.[31, 34-36] The preliminary results with the HDPE and LLDPE butene copolymer (Fig. 4.5) show that backbone segments with $^{13}C$ signals at 33 ppm and 31 ppm contribute to the intermediate mobility observed in the $^{1}H$ single-pulse spectra.

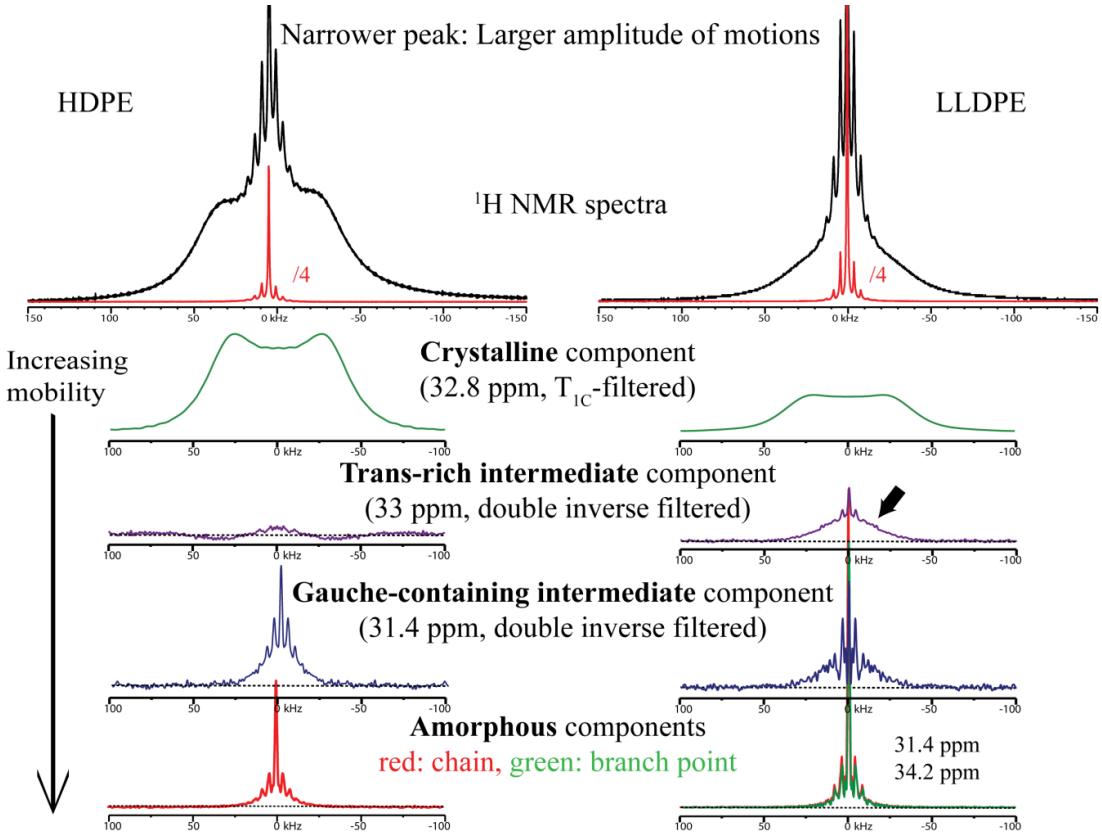


**Figure 4.5**. Preliminary spectra from WISE experiments on HDPE and LLDPE, compared to $^{1}H$ single-pulse spectra

Goldman-Shen Spin Diffusion

This Goldman-Shen spin diffusion experiment was implemented as a one-dimensional variation of the WISE experiment. Because the initial $^{13}C$ magnetization is destroyed by the pulse train at the beginning of the experiment (Fig 4.4b) the only signal observed in the $^{13}C$ spectrum should be coming from the cross-polarization from $^{1}H$. After the initial polarization of $^{1}H$, a $T_{1\rho H}$ filter is used to suppress the signal of all $^{1}H$ nuclei but those on the fastest-moving segments. By varying the length of the spin diffusion period, the distance between the most mobile $^{1}H$ nuclei and the $^{13}C$ species that appear in each successive $^{13}C$ spectrum can be established.[37] Incorporation of the same spectral editing techniques is informative in these experiments as well, in order to reveal any differences in localization of segments with differing mobility.

Dephasing by Chemical Shift Anisotropy

The chemical shift anisotropy (CSA) dephasing experiment selectively dephases the signal of $^{13}C$ nuclei located in segments that change orientation slowly on the time scale of the inverse of the frequency associated with the chemical-shift anisotropy.[38] This experiment was combined with $T_{1C}$ filtering in CP-based experiments to probe the relative mobility of the more-rigid components that appear in the $T_{1C}$ filtered CP spectrum.

## Specific Study Questions

With the experiments described above, we were able to address the following more specific questions for the ethylene-hexene copolymers, based on the general questions listed in Chapter 1:

1. What are the dynamic and conformational properties of the component revealed by the double inverse filter?
2. Do the butyl branches appear in this component, and if so, to what degree? How do their dynamic and conformational properties compare to branches in other components of the phase structure?
3. Where is the component revealed by the double inverse filter located within the lamellar structure? Does it really correspond to the interfacial region or "interphase"?
4. What fraction of the polymer material does the component revealed by the double inverse filter represent?

The answers based on our experimental results are given in Chapter 5.

# CHAPTER 5: BUTYL BRANCH LOCATION AT THE CRYSTAL SURFACE IN POLYETHYLENES DETECTED BY NMR

Modified from a paper to be submitted to *Macromolecules*

Allison White[1], Kanmi Mao[2], Diana Smirnova[2], Klaus Schmidt-Rohr[1,3]

1: Department of Chemistry, Iowa State University, Ames, IA 50011, USA
2: ExxonMobil Research & Engineering Company, Annandale, NJ 08801, USA
3: Department of Chemistry, Brandeis University, Waltham, MA 02453, USA

## Experimental

### Sample Origin and Preparation

Ethylene-hexene copolymers were provided by Exxon Mobil Research & Engineering Company (EMRE). In this manuscript, the samples are named according to their comonomer content and molecular weight; e.g., "PE-h0.9L" indicates a polyethylene prepared with hexene (0.9 mol%) that has lower molecular weight than other h0.9 samples.

The samples were provided as the ends of dogbone-shaped tensile test specimens approx. 3.5 mm thick. Using a 1/4-inch punch and an arbor press, disks measuring 5.3-5.5 mm in diameter were cut from the dogbone-shaped specimens. This diameter ensures a snug fit in 7-mm MAS NMR rotors (5.5-mm inner diameter). Loading the rotor with snugly-fitting disks maximizes the fill factor.

### Solid-State NMR

The solid-state magic angle spinning (MAS) NMR studies were carried out on a Bruker 400 MHz spectrometer at a $^{13}C$ frequency of 100 MHz. A 7-mm MAS probehead was used to maximze signal per scan, with 4 kHz magic angle spinning

and high-power $^{1}H$ decoupling. Direct-polarization (DP) and cross-polarization from $^{1}H$ (CP) spectra were measured with 4- 4.4-μs 90° pulses and 60 kHz TPPM decoupling. All spectra were recorded with a Hahn spin echo before detection to avoid baseline distortions by pulse dead time. For both CP and DP spectra, spectral-editing pulse sequences were used to selectively retain or suppress signals from the polymer backbone or branch segments with certain dynamics or structural characteristics.

**Standard and Inverse $^{13}C$ $T_1$ Filtering**

The spin-lattice relaxation time $T_{1C}$ of $^{13}C$ in crystalline polyethylene is very long (>100 s), while the $T_{1C}$ of amorphous polyethylene (~0.4 s) is orders of magnitude shorter.[12] Therefore, the signals of the crystalline segments can be obtained selectively in a CP experiment by storing the magnetization along the ±z direction for > 1 s (this period is referred to as the $T_{1C}$ filter), which is > 2 $T_{1C}$ of the amorphous segments.

As a complement to the normally filtered spectrum, an inverse-filtered spectrum can be calculated as the difference between the corresponding unfiltered (total) and filtered spectra. [39, 40] The result of this operation is a spectrum consisting of all of the intensity that was removed by the filter – in the case of $T_{1C}$ relaxation, the inverse-filtered spectrum selectively shows the signals of the $^{13}C$ species that have short $T_{1C}$. The filtered and inverse-filtered spectra together contain all of the intensity from the original total spectrum.

The inverse $T_{1C}$-filtered CP spectrum is similar to the spectrum obtained in a DP experiment with a recycle delay ≤ 2 s, which is an insufficient length time

between scans for $T_{1C}$ relaxation to regenerate the slowly relaxing signal from the crystalline segments of the polymer. [40] After hundreds of scans, the signal of crystalline segments becomes suppressed. It follows that DP spectra (with sufficiently short recycle delays) selectively show the intensity associated with noncrystalline $^{13}C$ nuclei, which have short $T_{1C}$. Therefore all of the 2-s recycle delay DP spectra shown below inherently include an inverse $T_{1C}$ filter.

**Standard and Inverse Dipolar Dephasing**

Spectral editing based on the $^{13}C$-$^{1}H$ dipolar coupling (dipolar dephasing) is made possible because the dipolar coupling is averaged by fast large-amplitude motions. In both the CP and DP dipolar dephasing experiments, a period of 40 μs without $^{1}H$ decoupling is included in the pulse sequence just before acquisition. This dipolar dephasing period is just long enough to suppress signals from immobile C-H groups with strong $^{13}C$-$^{1}H$ dipolar couplings, while retaining signals from mobile $^{13}C$ nuclei with relatively weak $^{13}C$-$^{1}H$ dipolar couplings. After 40 μs, >90% of signals from non-protonated carbons are retained, and, more importantly for PEs, large fractions of the signals of highly mobile segments in the noncrystalline regions are still observed. The signals of methyl groups, which only undergo rotational motions around the $C_3$ symmetry axis without significant motion of the $C_3$ axis itself, dephase to about 60% of their original intensity. Therefore, a standard dipolar-dephased DP or CP spectrum shows the signals of $^{13}C$ nuclei in more-mobile segments. The inverse dipolar-dephased DP or CP spectrum, calculated as the difference between the total and filtered spectra, shows the signals of $^{13}C$ nuclei in less-mobile segments.

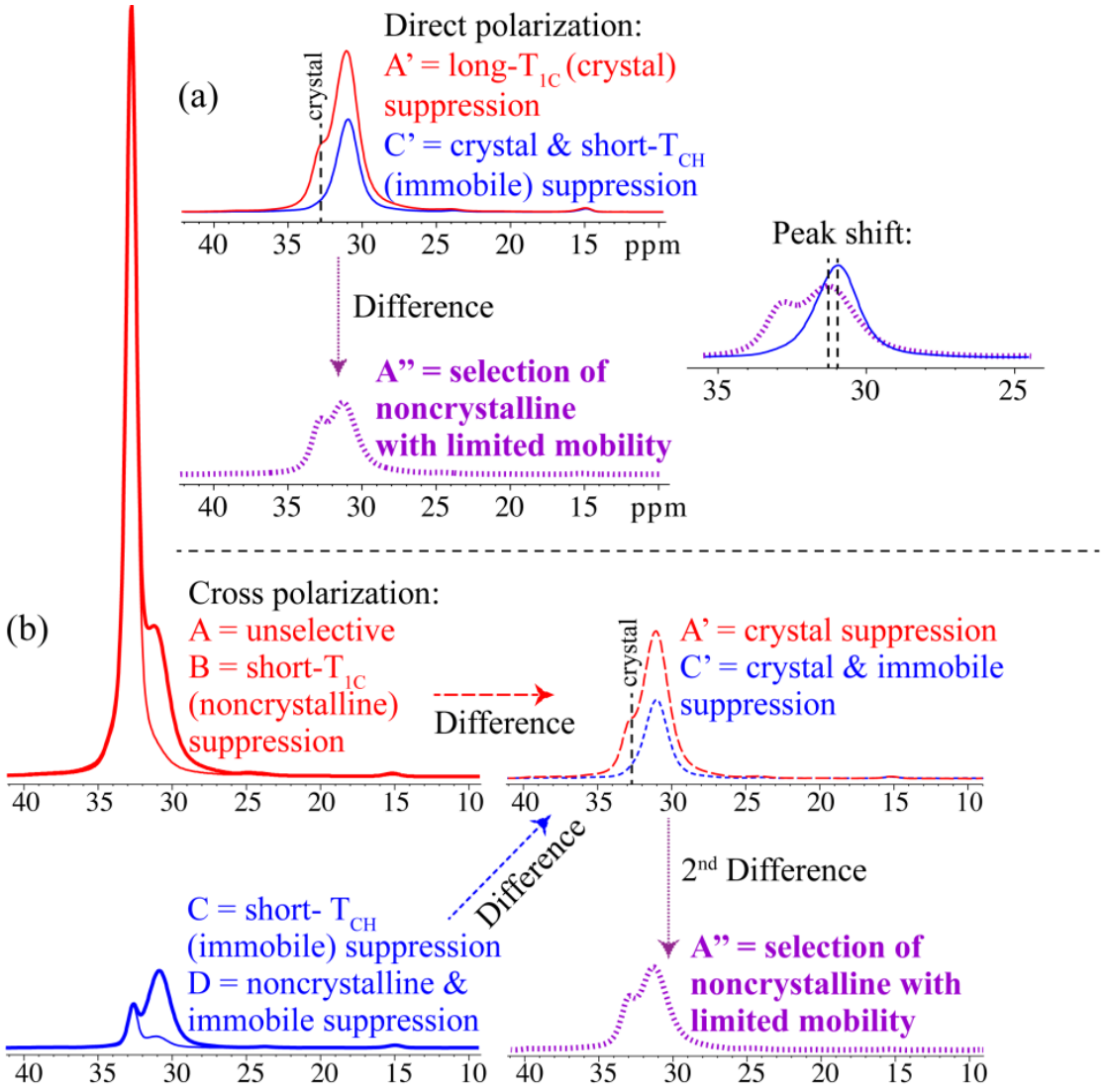


**Figure 5.1.** Principle of double inverse filtering demonstrated on PE-h0.9L using (a) direct polarization and (b) cross polarization from $^{1}H$; measured spectra are indicated by solid lines, spectra obtained by difference are indicated with dashed lines; a) DP with 2-s recycle delay (A', red trace), DP with 2-s recycle delay and 40-μs dipolar dephasing (C', blue trace), difference between A' and C' (A''), comparison between C' and A'' (side panel); b) CP (A, thick red trace), CP with 2-s $T_{1C}$ filter (B, thin red trace), CP with 40-μs dipolar dephasing (C, thick blue trace), CP with 40-us dipolar dephasing and 2-s $T_{1C}$ filter (D, thin blue trace), difference between A and B (A'), difference between C and D (C'), difference between A' and C' (A'')

**Double Inverse Filtering**

Inverse $T_{1C}$ filtering and inverse dipolar dephasing can be combined to select the signals of noncrystalline segments (with short $T_{1C}$) that have limited mobility (short $T_{CH}$). We refer to this as double inverse filtering. Two implementations are demonstrated and explained in Figure 5.1.

In Figure 5.1a, signals with short $T_{1C}$ are selected simply by direct polarization with a short (2-s) recycle delay (spectrum A'). This selection is followed by inverse dipolar dephasing: subtracting the dipolar-dephased spectrum (C') from A' to give A'', a double inverse filtered spectrum that selectively shows the noncrystalline segments with limited mobility. The side panel of Figure 5.1a shows that the double inverse filtered spectrum (A'') of limited-mobility noncrystalline segments is distinct from the dipolar-dephased and inverse $T_{1C}$ filtered spectrum (C') of the mobile noncrystalline segments. The shift in the peak maximum (Figure 5.1a, right hand side) confirms that this approach has selected a distinct structural component.

The simple direct-polarization approach cannot be applied to experiments that take advantage of $^1$H-based observables, such as $T_{1\rho H}$ measurement or $^1$H spin diffusion. For these experiments, we need to implement double inverse filtering after the cross polarization from $^1$H. Figure 5.1b shows how this can be achieved, based on four measured spectra: full unfiltered (A), after $T_{1C}$ filter (B), after dipolar dephasing (C), and after dipolar dephasing and $T_{1C}$ filter (D). The difference between A and B is an inverse $T_{1C}$-filtered spectrum (A') showing only the noncrystalline segments, while the difference between C and D is an dipolar-dephased and inverse

$T_{1C}$-filtered spectrum (C') showing only the mobile noncrystalline segments. These two spectra (A' and C') are shown in the upper right panel of Figure 5.1b and correspond to the two spectra measured in the DP approach, except for some intensity changes due to differential cross-polarization efficiency. The difference between these two spectra, as in the DP approach, is a double inverse filtered spectrum (A'') that selectively shows the limited-mobility noncrystalline segments, which are distinct from the mobile noncrystalline segments.

The double inverse filtering approach is robust and reproducible, in particular since it does not rely on adjustable scaling factors. With CP, it is advisable to signal average in blocks, i.e. repeat all four experiments in a loop, so that slow drifts in the CP condition and signal phase are reflected similarly in each of the four spectra and do not result in spurious difference signals.

**Experiments With $^1$H-Based Observables**

The Goldman-Shen spin diffusion[37, 41] experiment is used to identify the location of certain types of segments within the lamellar phase structure. Experiments run at 4-kHz MAS begin with selection of the $^1$H magnetization of the most mobile segments by a $T_{2H}$ filter of 250 μs duration (with the radio-frequency pulses on resonance). During a subsequent mixing time, which can be varied between 0.05 and 500 ms, the magnetization is stored along the ±z direction and $^1$H spin diffusion occurs, first to the directly neighboring and later more distant segments, with diffusion coefficients of 0.1 – 0.8 nm$^2$/ms.[37] The resulting magnetization distribution is reflected in the spectrum recorded after a read-out pulse and 30-μs cross polarization to $^{13}$C.

Segments can also be localized in the phase structure by experiments that measure $^{1}H$ $T_{1\rho}$ dephasing.[42] Those experiments include a spin lock of ~ 5 ms followed by cross polarization and $^{13}C$ detection. While the spin lock scales down the $^{1}H$-$^{1}H$ dipolar couplings, $^{1}H$ spin diffusion still occurs and the $T_{1\rho}$ relaxation is averaged over a region of ~1 nm diameter. All of these experiments can be combined with double inverse filtering to select the limited-mobility noncrystalline segments.

**CSA Filtering**

A 5-period CSA (chemical-shift anisotropy) dephasing sequence is employed to probe segmental mobility.[38] Signals of segments which change orientation quickly on the time scale of the inverse of the chemical-shift anisotropy are retained in the spectrum. This experiment is combined with double inverse filtering to selectively observe the limited-mobility noncrystalline segments.

## Results and Discussion

**Distinct Branch Signals**

Figure 5.2a shows selective direct-polarization spectra of the mobile (thin line) and limited-mobility (thick line) noncrystalline components in PE-h0.9L. The latter are selected by double inverse filtering (for short $T_{1C}$ and $T_{CH}$) as described above. The main peaks of the backbone $CH_2$ groups near 31 and 33 ppm are seen in the bottom traces of Figure 5.2a. The doubly inverse filtered spectrum shows two main peaks, one of limited-mobility all-trans components at 33 ppm, and a band of limited-mobility gauche-containing segments near 31.2 ppm. The peak maximum of

the latter is shifted by +0.2 ppm relative to that of the highly mobile segments, indicating a slightly higher trans content in the limited-mobility segments.

Peaks of branch sites become discernible after 32-fold vertical expansion, top traces in Figure 5.2a, and can be observed with excellent signal-to-noise ratio. Near 25 ppm, signals of the near-terminal $CH_2$ group in the branch are observed. The spectra clearly show two components, a sharp peak of mobile branches at 24 ppm, and a less mobile component at 25 ppm. The signal at 25 ppm can be observed with less peak overlap after a $T_{1C}$ filter (Fig. 5.2b). Adding a strong CSA filter (dashed line Fig. 5.2b) further reduces the peak overlap due to preferential suppression of the backbone signal at 32.8 ppm.

Similar results are also found for copolymers with lower and higher hexene content (Fig. 5.3). The backbone signals show the same three components (limited-mobility all-trans, limited-mobility gauche-containing, and highly mobile) in somewhat different proportions. With the high hexene content, PE-h3.3, the sharp signal of mobile branches at 24 ppm is dominant, but after a $T_{1C}$ filter, the 25-ppm signal is still clearly visible. Conversely, with the 0.35-mol% hexene, PE-h0.35, the 24-ppm signal of mobile branches is barely visible.

**Immobilized-Branch Dynamics**

Limited mobility of the branch carbons resonating at 25 ppm is proven by the small amplitude of this peak after dipolar dephasing (Fig. 5.2, 5.3). Particularly noteworthy is the near-absence of the mobile-branch signal at 24 ppm in sample PE-h0.35 (Fig. 5.3d), which indicates that most branches in this sample are immobilized. This is fully consistent with the limited dipolar dephasing of the $CH_3$

intensity near 15 ppm in sample PE-h0.35 to ~55% in Figure 5.3d. This is essentially the value found in rigid solids, which confirms that almost all of the branches are immobilized.

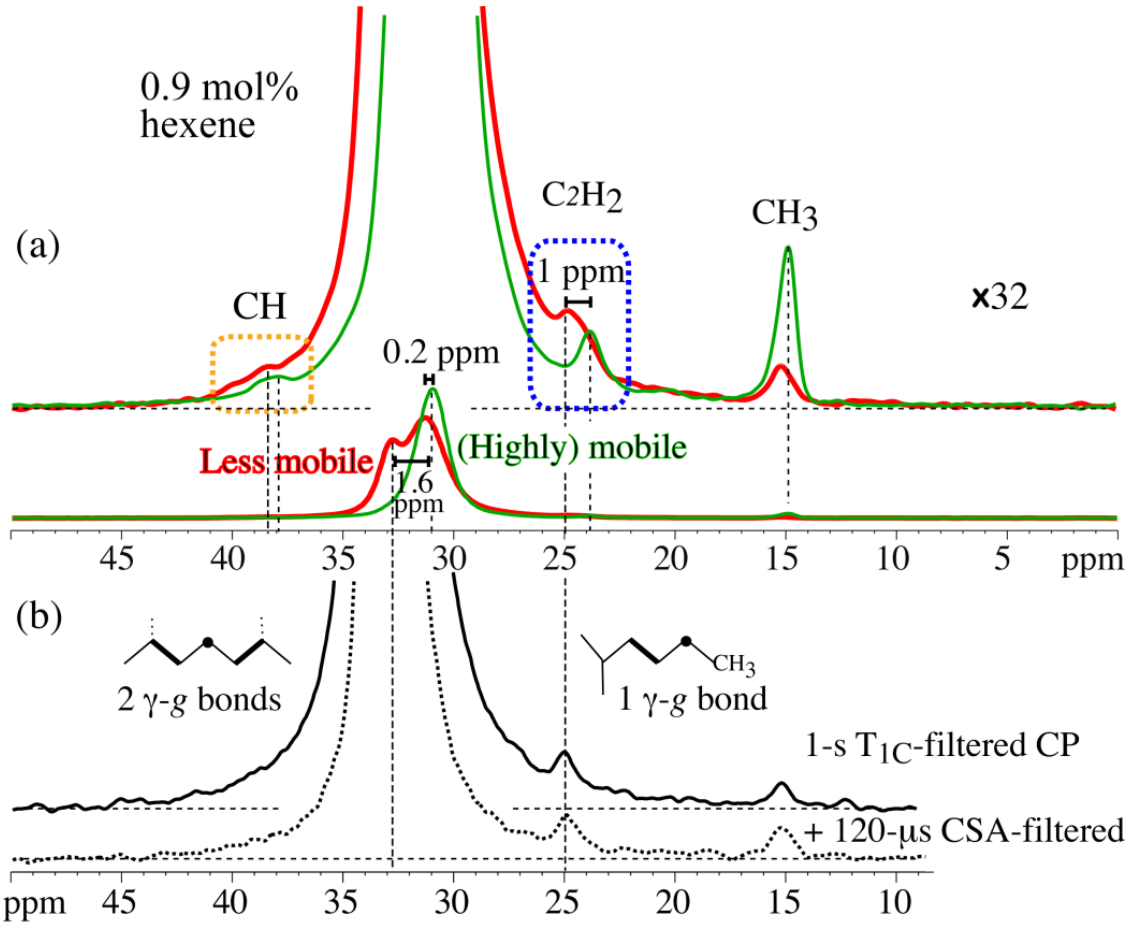


**Figure 5.2**. Spectra of PE with 0.9-mol% hexene comonomer PE-h0.9L; (a) DP spectra with 2-s recycle delays: dipolar-dephased (thin line) and inverse dipolar-dephased (i.e. double inverse filtered, thick line), full spectra (bottom traces) and 32-fold vertically expanded (top traces); (b) CP signals after a 2-s $T_{1C}$ filter (solid line) and with an additional 2-$t_r$ CSA filter (dashed line)

The limited mobility of the branch carbons resonating at 25 ppm is also confirmed by chemical-shift anisotropy dephasing, which is less pronounced for segments where fast (>$10^4$/s), large-amplitude motions average the chemical-shift anisotropy.[38] Figure 5.4(a) shows that 120-μs CSA dephasing reduces the 25-ppm signal to 24% of its original value. That is more pronounced CSA dephasing, corresponding to a smaller motional amplitude, than for the mobile branches resonating at 24 ppm, which dephase only to 82±8%. While the 24-ppm mobile branches show higher mobility than the backbone segments, as expected for the end of a sidegroup, the strong dephasing of the 25-ppm branches indicates their significant immobilization.

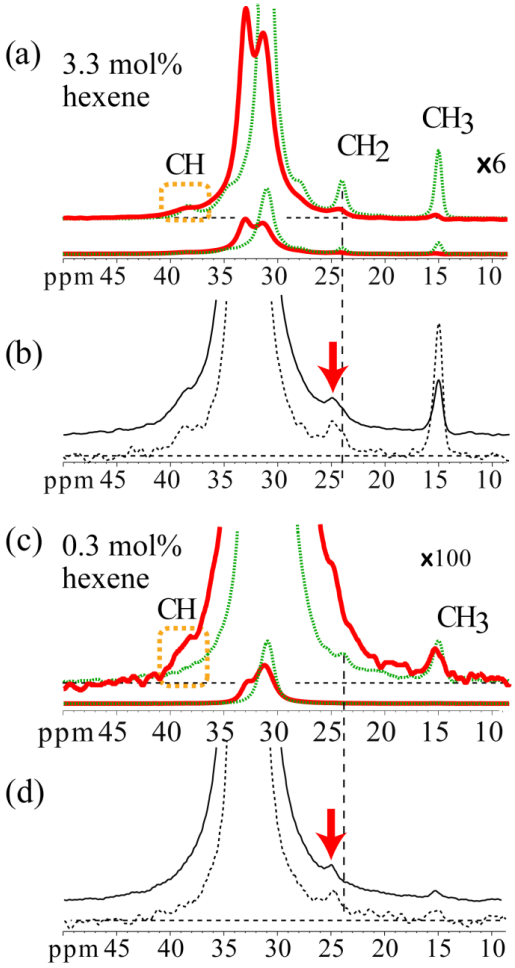


**Figure 5.3.** Spectra of PE with (a, b) 3.3-mol% (PE-h3.3) and (c, d) 0.35-mol% (PE-h0.35) hexene comonomer; (a, c) Selective DP spectra with 2-s recycle delays: dipolar-dephased (thin line) and inverse dipolar-dephased (i.e. double inverse filtered, thick line); (b, d) CP signals after a 2-s $T_{1C}$ filter (solid line) and with an additional 2-$t_r$ CSA filter (dashed line); full spectra (bottom traces) and vertically expanded (top traces) for each

**Immobilized-Branch Conformation**

Figure 5.2 highlights that the 1-ppm difference between the 24 and 25 ppm peak positions is much larger than the 0.2-ppm difference between the peak maxima, near 31 ppm, of the different gauche-containing noncrystalline components. While backbone $CH_2$ groups have at least two γ-carbons, the near-terminal $CH_2$ group (C2) resonating near 25 ppm has only one γ-carbon (i.e. a C at a three-bond distance) and therefore a smaller maximum γ-gauche shift.[10] Thus, the observed 1-ppm shift should effectively be doubled when comparing with that of backbone-carbons signals. It is therefore equivalent to the 2-ppm difference between the gauche-containing and all-trans backbone signals at 31 and 33 ppm, respectively. This suggests that the signal at 25 ppm corresponds to a mostly-trans C3-C4 bond in the immobilized branches.

The methyl signal of the immobilized branches is also shifted to the left relative to that of the highly mobile branches, but by a smaller amount, approximately +0.3 ppm. Through the γ-gauche effect, this C1 site probes the conformational statistics of the C2-C3 bond. The smaller γ-gauche shift indicates that this bond has a smaller trans population. The fast trans-gauche conformational exchange requires segmental mobility, which is qualitatively consistent with the reduced CSA dephasing of the C2 segment.

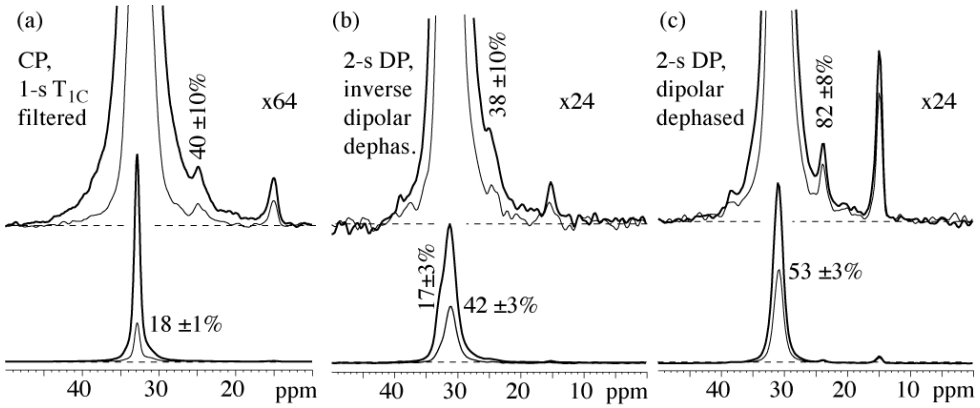


**Figure 5.4.** Selective $^{13}C$ NMR spectra, with corresponding CSA-dephased spectra; dephasing factors in Table S.1. Thick red line: signal after CSA dephasing with 120-μs periods, thin black line: signal with 1-ms periods for reference; spectra (a) with 2-s $T_{1C}$ filter before CP transfer and detection, selecting the long-$T_{1C}$ signal of the crystalline all-trans backbone carbons – the dephasing of the $CH_3$ signals must mostly be ignored here since they are not filtered like $CH_2$ and CH: the $CH_3$ has a longer $T_{1C}$, and therefore even noncrystalline $CH_3$ signals contribute after $T_{1C}$ filtering – (b) after double inverse filtering, selecting signals from limited-mobility noncrystalline segments with short $T_{1C}$ and $T_{CH}$; (c) after inverse $T_{1C}$ filtering with dipolar dephasing, selecting signals from highly mobile segments with short $T_{1C}$ and long $T_{CH}$

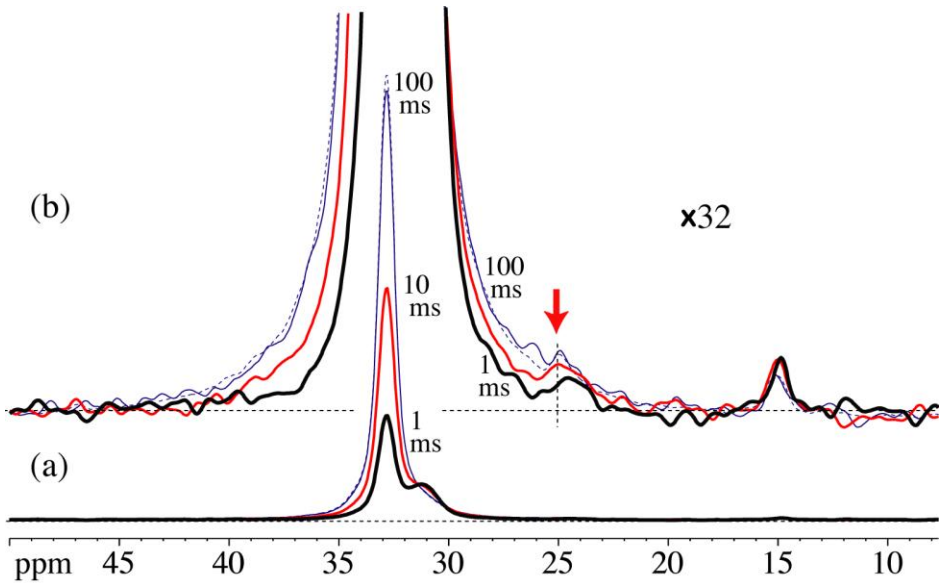


**Figure 5.5**. $^{1}H$ spin diffusion after $T_{2H}$ filtering and with $^{13}C$ NMR detection in PE with 0.9 mol% hexene; see Figure S.1 for an alternate presentation of this data. (a) Spectra after 1 ms (thick black bottom trace), 10 ms (middle trace) and 100 ms spin diffusion (thin blue top trace); (b) Same as (a) but expanded vertically by a factor of 32; the resolved signal of immobilized branches near 25 ppm is marked by an arrow; the thin dashed blue line is the unselective spectrum, corresponding to complete equilibration, after intensity matching with the spectrum after 100-ms spin diffusion

**Immobilized-Branch Location**

The location of the immobilized branches in the phase structure can be probed by $^1H$ spin diffusion. Selection of $^1H$ magnetization in mobile segments is achieved by a $T_{2H}$ filter and followed by spin diffusion of z-magnetization. If the immobilized branches are found in islands or clusters of immobilized segments in the noncrystalline regions, magnetization can reach them within ~1 ms. On the other hand, branches at the crystal surface are reached fully only on a 10-ms time scale. The series of spectra in Figure 5.5 shows that the magnetization of the 25-ppm peak has not equilibrated within 1 ms or even 10 ms, but keeps increasing almost like that of the crystal peak at 32.8 ppm. This similarity indicates that the branches resonating at 25 ppm are about as distant from the mobile core of the noncrystalline regions as the crystal is, i.e., those branches are located at the crystal surface.

$T_{1\rho H}$ relaxation can be used as an alternative branch-localization method. It is also based on $^1H$ spin diffusion but has a better signal-to-noise ratio than the Goldman-Shen experiment since it avoids the ~7-fold signal loss of the $T_{2H}$-selection step. In the noncrystalline regions, the spin locked magnetization decays with a significantly shorter time constant $T_{1\rho}$ than in the crystalline regions, due to significant spectral density of segmental dynamics near $\omega_1 = \gamma B_1 \sim 300{,}000/s$, where $B_1$ is the strength of the spin-lock field. During the spin lock time, $^1H$ spin diffusion occurs (though with a 2-4-fold reduced diffusion coefficient) and spreads the magnetization. Within a 5-ms spin-lock period, the $T_{1\rho}$ relaxation is spatially averaged over a region of ~1-nm diameter, in particular in regions with limited

motional averaging of $^{1}H$-$^{1}H$ dipolar couplings. Thus, the extent of $T_{1\rho}$ dephasing of the branches is indicative of their local environment.

Figure 5.6 shows 5-ms $^{1}H$ $T_{1\rho}$-relaxed spectra detected after $T_{1C}$ filtering, dipolar dephasing, and double inverse filtering. The full spectra displayed in the bottom rows for each sample highlight the distinct relaxation factors of the crystalline, limited-mobility all-trans, limited-mobility gauche-containing, and most mobile gauche-containing components, with values of 89, 77, 59, and 48%, respectively for PE-h0.9L. The branch signals at 24-25 ppm, made visible in the top rows of Figure 5.6 by vertical scaling, show similarly pronounced differences. In particular, the sharp, long-$T_{1C}$ signal at 25 ppm shows relatively little relaxation (to 80±10%), which is significantly different from that of the gauche-containing components (<60%). This is also mirrored (though with poorer resolution) by the relaxation of the CH signal near 39 ppm. The slow $T_{1C}$ and $T_{1\rho}$ relaxation of these signals strongly indicate a location of the corresponding branches in the all-trans crystal surface region of the phase structure.

Corresponding results are seen for other samples (Fig. 5.6). Samples PE-h0.9H and PE-h3.3, which have lower crystallinities, exhibit faster $T_{1\rho}$ relaxation, but again the relaxation of the long-$T_{1C}$, trans-rich branch at 25 ppm is comparable to that of the mobile or even of the crystalline trans backbone signals. It should be noted that the observed shorter $T_{1\rho}$ values of the noncrystalline segments in PE-h3.3 and PE-h0.9H relative to PE-h0.9L must be attributed to larger amplitudes of motion, rather than faster motions: Since the motional rates are faster than the minimum in the $T_{1\rho}$ dependence on rate, faster motions result in *longer* $T_{1\rho}$.

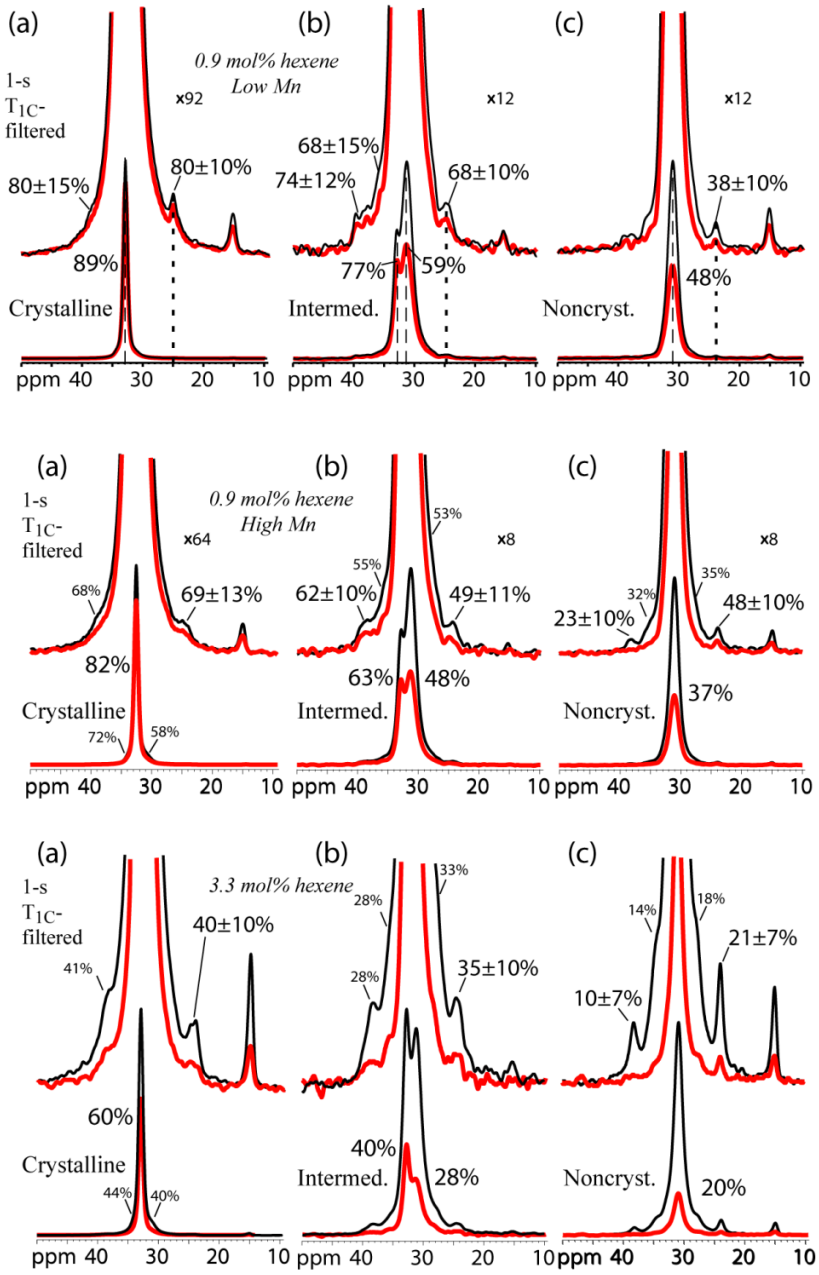


**Figure 5.6.** Selective $^{13}C$ NMR spectra probing $^{1}H$ $T_{1\rho}$ dephasing (thick line: after 5-ms spin lock; thin line: signal after only 0.02 ms for reference), before cross polarization from $^{1}H$ to $^{13}C$; from top to bottom: PE-h0.9L, PE-h0.9H, PE-h3.3. (a) with 1-s $T_{1C}$-filter before detection, which selects the long-$T_{1C}$ signal of the crystalline all-trans backbone carbons; (b) after double inverse filtering, selecting signals from limited-mobility noncrystalline segments with short $T_{1C}$ and $T_{CH}$. (c) after inverse $T_{1C}$ filtering of signals from mobile segments, with short $T_{1C}$ and long $T_{CH}$; the dephasing of the $CH_3$ signals must mostly be ignored here since they are not filtered like $CH_2$ and CH: the $CH_3$ has a longer $T_{1C}$, and therefore even noncrystalline $CH_3$ signals contribute after $T_{1C}$ filtering

**Immobilized-Branch Content**

Figure 5.7 shows 2-s $T_{1C}$ filtered spectra of six hexene copolymers vertically expanded to make the branch signals visible; the maxima of the peak at 32.8 ppm are scaled to match. While the comonomer content varies nearly 10-fold (which is reflected in the $CH_3$ signal intensity at 15 ppm), the intensity of the 25-ppm signal is approximately constant for the samples with 0.9 to 3.3 mol% hexene.

The absolute quantification of interfacial branch content based on the area of the branch signal relative to that of all $CH_2$ groups is challenging, due to peak overlap and different attenuation of branch and backbone signals by spectral filters. A more accurate estimate can be made based on the known branch fractions of the various polyethylenes studied. The spectra in Figure 5.2 and 5.3 show that the interfacial branches make up about 90% of all branches in sample PE-h0.35 and about 2/3 in sample PE-h0.9L. These values correspond to 0.3 - 0.6 mol% $C_2H_3R$ (i.e., 3-6 immobilized branches per 2000 C). Below, we will show that this is consistent with these branches being located near the crystal surface.

The spectra in Figure 5.7 show recognizable differences in the width of the 25-ppm peak. Smaller line widths are observed for lower molecular weights $M_n$, indicating that a higher degree of conformational order can be achieved for smaller $M_n$.

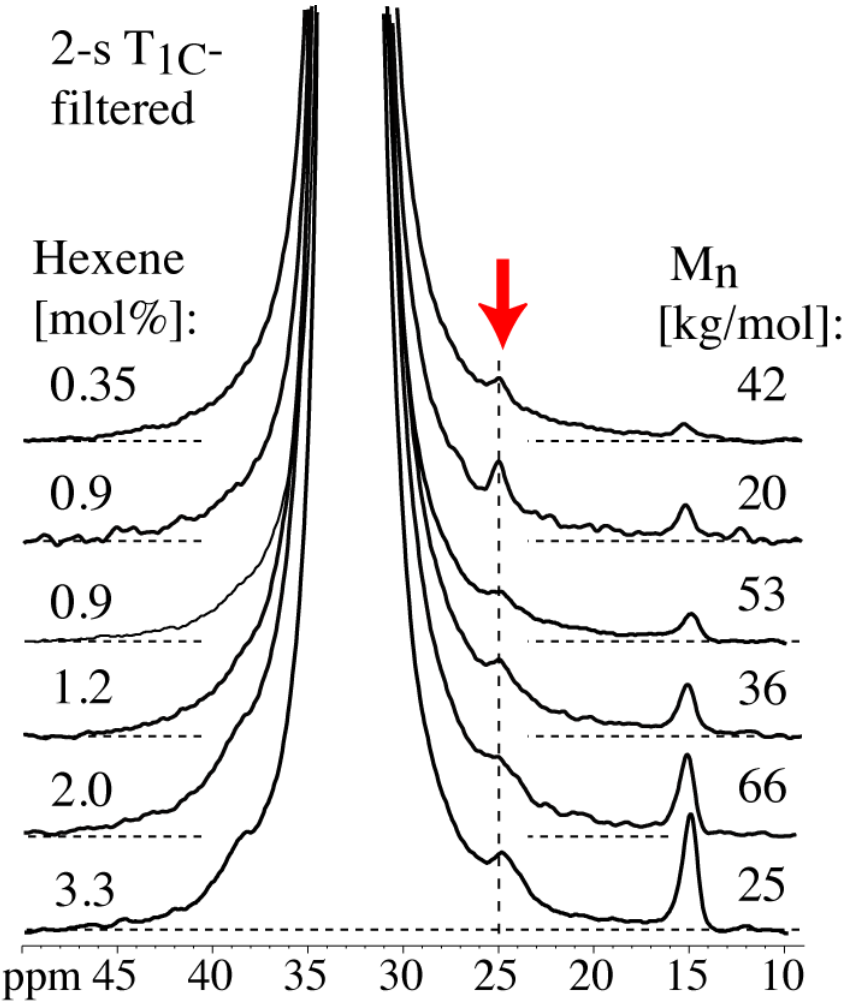


**Figure 5.7**. Series of 2-s $T_{1C}$ filtered spectra of polyethylenes with increasing hexene content (by nearly 10-fold) from top to bottom; the maxima of large crystalline-$CH_2$ peaks at 32.8 ppm were scaled to the same height

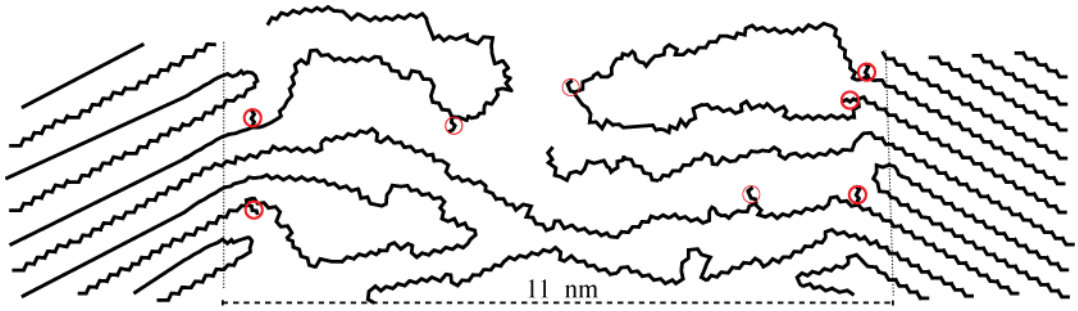


**Figure 5.8.** Model of an amorphous region and parts of adjacent crystalline lamellae in PE-h0.9L, with the butyl branches highlighted by red circles; with 13-nm thick crystals, the mass crystallinity of the model is 63%, and the volume crystallinity 59%. The full morphological repeat unit of the model contains 1700 $CH_2$ units and 15 branches, i.e. 0.9 mol% branches; based on the NMR evidence, branches are shown preferentially near the crystal surface (0.5 mol%)

**Structural Model and Fraction of Crystal-Surface Sites[8]**

Based on the NMR data presented here and layer thicknesses from SAXS analysis, we propose a model where branches are located at the crystal surface to the extent permitted by their random placement along the PE backbones (Fig. 5.8). The figure shows that the fraction of such surface sites is very small. The model has only 4 interfacial branches out of 900 $CH_2$ units (0.5 mol%) in the morphological repeat (of which the branch-free crystal layers are only partially shown in the figure). A stem traversing the crystal can have a branch at both interfaces only if the branch spacing matches the stem length, which is not common. Therefore, the figure shows only about half the interfacial sites with a branch. Additional branches are mostly forced into the interior of the noncrystalline regions based on their location along a chain, as seen, for instance, in the center right chain in Figure 5.8.

**Table 5.1.** Determination of the percent of limited-mobility gauche-containing intermediate in each polyethylene-hexene copolymer sample. DD: dipolar-dephased spectrum, invDD: inverse dipolar-dephased spectrum, ATI: all-trans intermediate, GCI: gauche-containing intermediate; all given as the percentage of the intensity of the full spectrum. $x_i$: given as the percentage of the phase structure (see Table 2.1). More extensive description of calculations and abbreviations in Table S.3

| Sample | DD | invDD | ATI | GCI | Limited-mobility GCI<br>% of GCI | $x_a$ | Limited-mobility GCI<br>% of structure |
|---|---|---|---|---|---|---|---|
| PE-h0.35 | 50.5 | 49.4 | 11.0 | 88.9 | 43.2 | 38 | 16.4 |
| PE-h0.9L | 44.8 | 55.2 | 15.8 | 84.2 | 46.8 | 45.4 | 21.2 |
| PE-h0.9H | 51.5 | 48.5 | 13.4 | 86.6 | 40.5 | 56.6 | 22.9 |
| PE-h1.2 | 51.0 | 49.0 | 14.3 | 85.7 | 40.5 | 55.9 | 22.6 |
| PE-h2.0 | 55.0 | 45.0 | 14.7 | 85.3 | 35.5 | 61.5 | 21.8 |
| PE-h2.3 | 56.7 | 43.3 | 14.6 | 85.4 | 33.6 | 60.9 | 20.5 |
| PE-h2.8 | 57.2 | 42.8 | 14.9 | 85.1 | 32.8 | 61.4 | 20.1 |
| PE-h3.3 | 54.8 | 45.2 | 18.1 | 81.9 | 33.1 | 57.4 | 19.0 |
| PE-h4.4 | 57.7 | 42.3 | 17.6 | 82.4 | 30.0 | 55.9 | 16.8 |

The analysis shows that only one branch per crystal stem or equivalently per average morphological repeat can freely be located at the crystal surface. SAXS shows that the morphology has a repeat thickness of 24 nm. The projected length of the chain per $C_2H_4$ is ~0.2 nm (considering chain tilt), so there are 25 nm / 0.2 nm = 125 $C_2H_4$ groups in a typical chain traversing the morphological repeat. One $C_2H_3R$ comonomer unit located where the chain emerges from the crystal corresponds to 1/125= 0.8 mol%. Thus, the expected level of interfacial branches is at most 0.8 mol%. This is compatible with the fraction of immobilized branches estimated above from our NMR data. The model structure of Figure 5.8, corresponding to a morphological repeat unit of one noncrystalline layer and two half crystal layers (which are only partially shown), has 5/900 = 0.55 mol% interfacial branches.

**Interfacial Branches and Chain Diffusion.**

Chain diffusion[43] due to chain displacements accompanying chain flips in the crystallites[44-46] has significant implications for the macroscopic mechanical and microscopic structural properties of polyethylenes. In the HDPE and LLDPE materials studied here, chain diffusion enables the movement of the branches to thermodynamically favored locations. Conversely, branches near the interface must severely limit displacements due to chain diffusion. The branch cannot move into the crystal, and if it is located at the crystal surface it generally does not move far from the crystal.

It has been shown that chain diffusion can be probed by $T_{1C}$ relaxation of the crystalline component, since chain diffusion results in the transport of magnetization into the crystal from the fast-relaxing noncrystalline segments, with nonexponential character[43]. Consequently, the restriction of chain diffusion in branched PEs to a limited fraction of segments near the crystal surface should be reflected in the $T_{1C}$ relaxation curve. Chain diffusion would result in fast relaxation of a limited fraction of crystalline components. When further chain diffusion is stopped by the branches, a distinct switch to slower, more exponential relaxation by other mechanisms will occur.

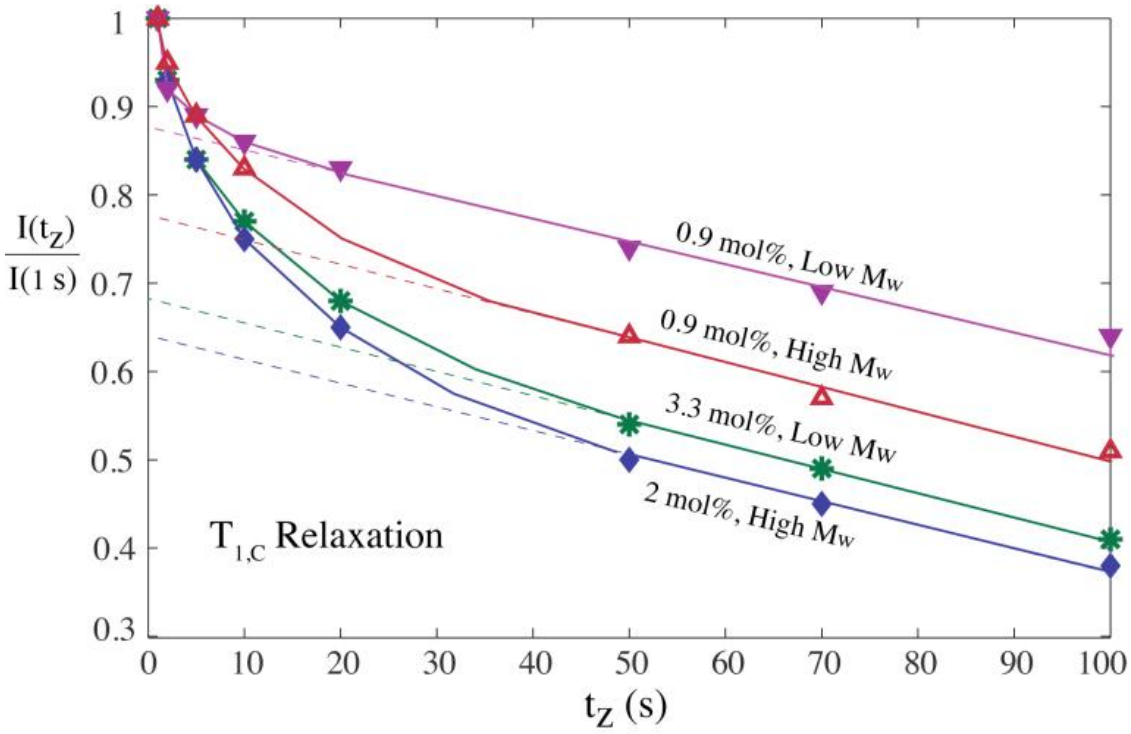


**Figure 5.9.** $T_{1C}$ relaxation curves for the crystalline signal at 32.8 ppm, of four HDPE-hexene copolymers, at 300 K: the intensity is normalized to the value at 1 s, when most of the noncrystalline background has disappeared; comparison of the data of PE-h0.9L vs. PE-h0.9H and of PE-h3.3 vs. PE-h2 is particularly instructive

This is indeed observed in the experimental data shown in Figure 5.9, most clearly for PE-h0.9L. Only about 12% of the crystalline segments undergo fast relaxation on the 3-s time scale, which we attribute to chain diffusion. For PE-h0.9H, the fast-relaxing fraction is higher at about 22%, consistent with the less ordered structure near the interface deduced from the $^{13}C$ NMR line width. Only a small part of this difference, about 2% of the 22 vs. 12% difference, can be attributed to the smaller crystal thickness $L_c$ of PE-h0.9H (Table 2.1).

On the other hand, the crystal-thickness difference explains most of the larger fast-dephasing fraction of PE-h2. In a thinner crystal, a surface layer of given thickness accounts for a larger fraction of segments. Quantitatively, 22% of the 11.2-nm $L_c$ of PE-h0.9H is 2.5 nm, which corresponds to 2.5/8 = 31% of the 8-nm Lc of PE-h2 and thus explains most of the 36% fast-relaxing component seen in Figure 5.8. The correlation of a higher degree of order in the interfacial branches with a smaller fast-relaxing, chain-diffusion component is again observed when comparing the relaxation behavior of PE-h3.3 with that of PE-h2.

In both pairs of samples in Fig. 5.9, lower Mw correlates with a smaller fast-relaxing component. We attribute this to reduced chain diffusion due to more ordered location of branches closer to the crystal surface for the less entangled shorter chains.

Supplemental information included in Appendix A.

# CHAPTER 6: CONCLUSIONS

## Summary

Preliminary experiments with an HDPE and ethylene-butene copolymer demonstrated the $^{1}H$ and $^{13}C$ NMR characteristics of the crystalline-noncrystalline interface, so that its signals could be isolated through the spectral editing technique referred to as double inverse filtering.

The signals of interfacial segments of ethylene-hexene copolymers were selected by double inverse filtering, and it became apparent that a fraction of the branches in every sample tested fell within the regime selected by that spectral editing process (less mobile noncrystalline material).

The conformation of the less mobilie branches was characterized by examining the change in chemical shift for the same segment in different $T_{1C}$- and $T_{CH}$- selective spectra. This shift was attributed to the gamma-gauche effect and showed that less mobile branches have a higher trans/gauche ratio. The amplitude of motion of the branches was characterized by applying CSA dephasing to the selective spectra, which showed that the trans-rich less mobile branches also have smaller motional amplitudes. The interfacial location of the less mobile branches was established using spin diffusion combined with a double inverse filter as well as $^{13}C$ spectra with $T_{1\rho}$ dephasing. The $T_{1C}$ of several components was measured and the consequences with respect to chain diffusion were discussed.

## Future Directions

The results of this study clarified some questions about short branches in LLDPE, but there is much more to be determined about the relationship between the composition, microstructure, phase structure, and physical properties of PE copolymers. Future directions for this research must include continued efforts to reconcile structural models with physical properties through carefully designed experimental studies of well-defined PE materials. NMR can play a key role in this process by probing the structure and dynamics of the polymer backbone and branches within and between the crystalline lamellae.

One potential extension of the investigation of interfacial region could take advantage of an experimental strategy developed by the Harris group. Recently published as CLASSIC NMR (Combined Liquid- And Solid-State In-situ Crystallization NMR), their method consists of alternating two experiment types to collect selective spectra of solid and liquid components, respectively, over time as a solution crystallizes.[47] They describe how this can be done in a normal solid-state MAS probe. A version of this technique could be used to observe NMR properties of PE molecules as they crystallize. The double inverse filter, or a similar strategy requiring less time per round of experiments, could be applied to selectively observe the interfacial region during crystallization. This would complement existing non-NMR in-situ studies of the crystallization process, and could inform computational modeling of the process.

Another step forward would be to extend the principal experiments used in this project to other copolymers of PE in order to more systematically explore the effects of bulk density and molecular weight on the segments selected by the double inverse filter. Branch length, a parameter held constant in this study, could also be varied. I predict that these factors would correlate not only to the amount, conformation, and localization of the limited-mobility branches, but also to the lamellar width and interlamellar distance.

The double inverse filtering technique to isolate the signal from less mobile noncrystalline segments and branches should be applicable to other systems as well. Lamellar morphology would not be required for this technique to be useful; any system in which a tail or chain is emerging from a crystalline (or relatively rigid and ordered) surface could benefit from the ability to obtain spectra of only the less-mobile noncrystalline segments without overlap from the crystalline signal. This strategy could be useful for ssNMR studies of surfaces or nanoparticles decorated with organic molecules, for example, as well as for other semicrystalline polymers.

REFERENCES

1. John, The Big 6 Plastics. In It's The Rheo Thing, 2014; Vol. 2014.

2. Designer plastics. The Economist Technology Quarterly Dec 8, 2001, 2001, pp 26-28.

3. Tullo, A. H., α-Olefins Producers Ready Big Plants. Chemical & Engineering News 2014.

4. Peacock, A., Handbook of Polyethylene: Structures, Properties, and Applications. Marcell Dekker: New York, 2000.

5. Bunn, C. W. Transactions of the Faraday Society 1939, 35, 482-491.

6. Adams, W. W.; Briber, R. M.; Sherman, E. S.; Porter, R. S.; Thomas, E. L. Polymer 1985, 26, 17.

7. Capaccio, G.; Ward, I. M. Polymer 1974, 15, 233-238.

8. Baker, A. M. E.; Windle, A. H. Polymer 2001, 42, 667-680.

9. Albrecht, T.; Strobl, G. Macromolecules 1995, 28, 5827-5833.

10. Tonelli, A. E.; Schilling, F. C. Accounts of Chemical Research 1981, 14, 233-238.

11. Tonelli, A. E. Journal of Molecular Structure 1995, 355, 105-119.

12. Axelson, D. E.; Mandelkern, L.; Popli, R.; Mathieu, P. Journal of Polymer Science: Polymer Physics Edition 1983, 21, 2319-2335.

13. Axelson, D. E., Carbon-13 Solid-State NMR of Semicrystalline Polymers. In High Resolution NMR Spectroscopy of Synthetic Polymers in Bulk, Komoroski, R. A., Ed. VCH Publishers, Inc.: Deerfield Beach, Florida, USA, 1986; Vol. 7, pp 157-226.

14. Chen, Q.; Yamada, T.; Kurosu, H.; Ando, I.; Shiono, T.; Doi, Y. J. Mol. Struct. 1991, 263, 319-327.

15. Cheng, J.; Fone, M.; Fu, Y.; Chen, W. Journal of Thermal Analysis 1996, 47, 673-683.

16. Earl, W. L.; VanderHart, D. L. Macromolecules 1979, 12, 762-767.

17. Newman, R. The Journal of Chemical Physics 1950, 18, (9), 1303-1304.

18. Rempel, R.; Weaver, H.; Sands, R.; Miller, R. Journal of Applied Physics 1957, 28, (10), 1082-1089.

19. Wilson, C. W.; Pake, G. E. Journal of Chemical Physics 1957, 27, 115-122.

20. Hu, W. G.; Schmidt-Rohr, K. Polymer 2000, 41, 2979-2987.

21. Adams, W. W.; Yang, D.; Thomas, E. L. J. Mater. Sci. 1986, 21, 2239-2253.

22. Attenburrow, G. E.; Bassett, D. C. J. Mater. Sci. 1977, 12, 192-200.

23. Barham, P. J.; Arridge, R. G. C. J. Polym. Sci., Polym. Phys. Ed. 1977, 15, 1177-1188.

24. Young, R. J.; Bowden, P. B.; Ritchie, J. M.; Rider, J. G. J. Mater. Sci. 1973, 8, 23-26.

25. Bowden, P. B.; Young, R. J. Journal of Materials Science 1974, 9, 2034-2051.

26. Brooks, N. W.; Duckett, R. A.; Ward, I. M. Polymer 1992, 33, 1872-1880.

27. Chen, W.; Fu, Y.; Wunderlich, B.; Cheng, J. J. Polym. Sci. Part B: Polym. Phys. 1994, 32, 2661-2666.

28. Darras, O.; Seguela, R. Journal of Polymer Science: Part B: Polymer Physics 1993, 31, 759-766.

29. Cheng, J.; Fone, M.; Reddy, V. N.; Schwartz, K. B.; Fisher, H. B.; Wunderlich, B. Journal of Polymer Science: Part B: Polymer Physics 1994, 32.

30. Abragam, A., The Principles of Nuclear Magnetism. Oxford University Press Inc.: New York, 1961.

31. Schmidt-Rohr, K.; Spiess, H. W., Multidimensional Solid-State NMR and Polymers. Academic Press, Inc.: San Diego, 1994.

32. Bennett, A. E.; Rienstra, C. M.; Auger, M.; Lakshmi, K. V.; Griffin, R. G. Journal of Chemical Physics 1995, 103, 6951-6958.

33. Doskocilová, D.; Schneider, B.; Jakes, J.; Schmidt, P.; Baldrian, J.; Hernandez-Fuentes, I.; Caceres Alonso, M. Polymer 1986, 27, 1658-1664.

34. Beckham, H. W.; Spiess, H. W. Macromolecular Chemistry and Physics 1994, 195, 1471-1482.

35. Kulik, A. S.; Beckham, H. W.; Schmidt-Rohr, K.; Radloff, D.; Pawelzik, U.; Boeffel, C.; Spiess, H. W. Macromolecules 1994, 27, 4746-4754.

36. Schmidt-Rohr, K.; Kulik, A. S.; Beckham, H. W.; Ohlemacher, A.; Pawelzik, U.; Boeffel, C.; Spiess, H. W. Macromolecules 1994, 27, 4733-4745.

37. Clauss, J.; Schmidt-Rohr, K.; Spiess, H. W. Acta Polymerica 1993, 44, 1-17.

38. Mao, J. D.; Schmidt-Rohr, K. Solid State NMR 2004, 26, 36-45.

39. Mowery, D.; Schmidt-Rohr, K. Polymeric Materials: Science and Engineering 2001, 85, 35-36.

40. Mowery, D. M.; Harris, D. J.; Schmidt-Rohr, K. Macromolecules 2006, 39, 2856-2865.

41. Eckman, R. R.; Henrichs, P. M.; Peacock, A. J. Macromolecules 1997, 30, 2474-2481.

42. VanderHart, D.; Perez, E. Macromolecules 1986, 19, (7), 1902-1909.

43. Schmidt-Rohr, K.; Spiess, H. W. Macromolecules 1991, 24, 5288-5293.

44. Boyd, R. H. Polymer 1985, 26, 323-347.

45. Boyd, R. H. Polymer 1985, 26, 1123-1133.

46. Hu, W. G.; Boeffel, C.; Schmidt-Rohr, K. Macromolecules 1999, 32, 1611-1619.

47. Hughes, C. E.; Williams, P. A.; Harris, K. D. Angewandte Chemie International Edition 2014, 53, (34), 8939-8943.

APPENDIX: SUPPLEMENTAL INFORMATION FOR CHAPTER 5

**Table S.1**. 4x120-μs CSA dephasing factors for the major signals appearing in 2-s $T_{1C}$-filtered spectra (illustrated in Fig. 5.4)

| | 33 ppm | 24-25 ppm | 15 ppm |
|---|---|---|---|
| sample | backbone | branch $C2H_2$ | chain end $CH_3$ |
| PE-h0.35 | 0.10 | 0.22 | 0.28 |
| PE-h0.9L | 0.09 | 0.24 | 0.37 |
| PE-h1.2 | 0.10 | 0.19 | 0.42 |
| PE-h2.0 | 0.09 | 0.18 | 0.47 |

**Table S.2**. Relaxation factors after 5-ms spin lock (illustrated in Fig. 5.6) for the major crystal, mobile amorphous, and constrained amorphous signals and branch signals

| sample | 38-40 ppm | | | 33 ppm | | 31 ppm | | | 24-25 ppm | | |
|---|---|---|---|---|---|---|---|---|---|---|---|
| | branch point CH | | | all-trans backbone | | gauche-containing backbone | | | branch $C2H_2$ | | |
| | rigid[a] | limited mobility[b] | highly mobile[c] | crystalline[a] | limited mobility[b] | rigid[a] | limited mobility[b] | highly mobile[c] | rigid[a] | limited mobility[b] | highly mobile[c] |
| PE-h0.9H | 0.68 | 0.62 | 0.23 | 0.82 | 0.63 | 0.58 | 0.48 | 0.37 | 0.69 | 0.49 | 0.48 |
| PE-h0.9L | -- | 0.74 | -- | 0.89 | 0.77 | -- | 0.59 | 0.48 | 0.80 | 0.68 | 0.38 |
| PE-h3.3 | 0.41 | 0.28 | 0.10 | 0.60 | 0.40 | 0.40 | 0.28 | 0.20 | 0.40 | 0.35 | 0.21 |

a: from $T_{1C}$-filtered (1 s) spectrum
b: from double inverse filtered spectrum
c: from inverse $T_{1C}$-filtered, dipolar-dephased spectrum

**Table S.3.** Full version of limited-mobility GCI table: (Table 5.1)
The percentages reported in the first three columns of the table were found by integrating the area under all (45-10 ppm) or part of the 40-μs dipolar-dephased ("DD", signal of more-mobile segments) or inverse dipolar-dephased ("invDD", signal of limited-mobility segments) DP spectrum for each sample, normalized to the area under the associated unfiltered 2-s recycle delay DP spectrum ("full"). The percent of gauche-containing intermediate (GCI) in the full spectrum is calculated by first finding the area of the all-trans intermediate (ATI) peak (35-32.3 ppm) in the invDD spectrum. That area is subtracted from the total area of the full spectrum to find the total amount of GCI. The area associated with ATI is also subtracted from the total area of the invDD spectrum to find the amount of limited-mobility GCI. The area associated with the limited-mobility GCI is divided by the total area associated with GCI to give the percent of all GCI segments that have limited mobility. That percent is multiplied by the value of the amorphous fraction in the sample to give the fraction of segments in the sample that are gauche-containing and have intermediate mobility, shown in the final column

| sample | mol% hexene | % DD vs "full" 45-10 ppm | % invDD vs "full" 45-10 ppm | % ATI (from invDD) vs "full" 35- ~32.2 ppm | % all GCI vs "full" | % more mobile GCI vs all GCI | % less mobile GCI vs all GCI | % amorphous in total phase structure (KM ssNMR) | % more mobile GCI in total phase structure | % less mobile GCI in total phase structure |
|---|---|---|---|---|---|---|---|---|---|---|
| E3 | 2.0 | 55.0 | 45.0 | 14.7 | 85.3 | 64.5 | 35.5 | 61.5 | 39.7 | 21.8 |
| D3 | 2.3 | 56.7 | 43.3 | 14.6 | 85.4 | 66.4 | 33.6 | 60.9 | 40.4 | 20.5 |
| C3 | 2.8 | 57.2 | 42.8 | 14.9 | 85.1 | 67.2 | 32.8 | 61.4 | 41.3 | 20.1 |
| B3 | 3.3 | 54.8 | 45.2 | 18.1 | 81.9 | 66.9 | 33.1 | 57.4 | 38.4 | 19.0 |
| A3 | 4.4 | 57.7 | 42.3 | 17.6 | 82.4 | 70.0 | 30.0 | 55.9 | 39.1 | 16.8 |
| D4 | 0.9 | 51.5 | 48.5 | 13.4 | 86.6 | 59.5 | 40.5 | 56.6 | 33.7 | 22.9 |
| C4 | 1.2 | 51.0 | 49.0 | 14.3 | 85.7 | 59.5 | 40.5 | 55.9 | 33.3 | 22.6 |
| D5 | 0.4 | 50.5 | 49.4 | 11.0 | 88.9 | 56.8 | 43.2 | 38 | 21.6 | 16.4 |
| B5 | 0.9 | 44.8 | 55.2 | 15.8 | 84.2 | 53.2 | 46.8 | 45.4 | 24.2 | 21.2 |

.

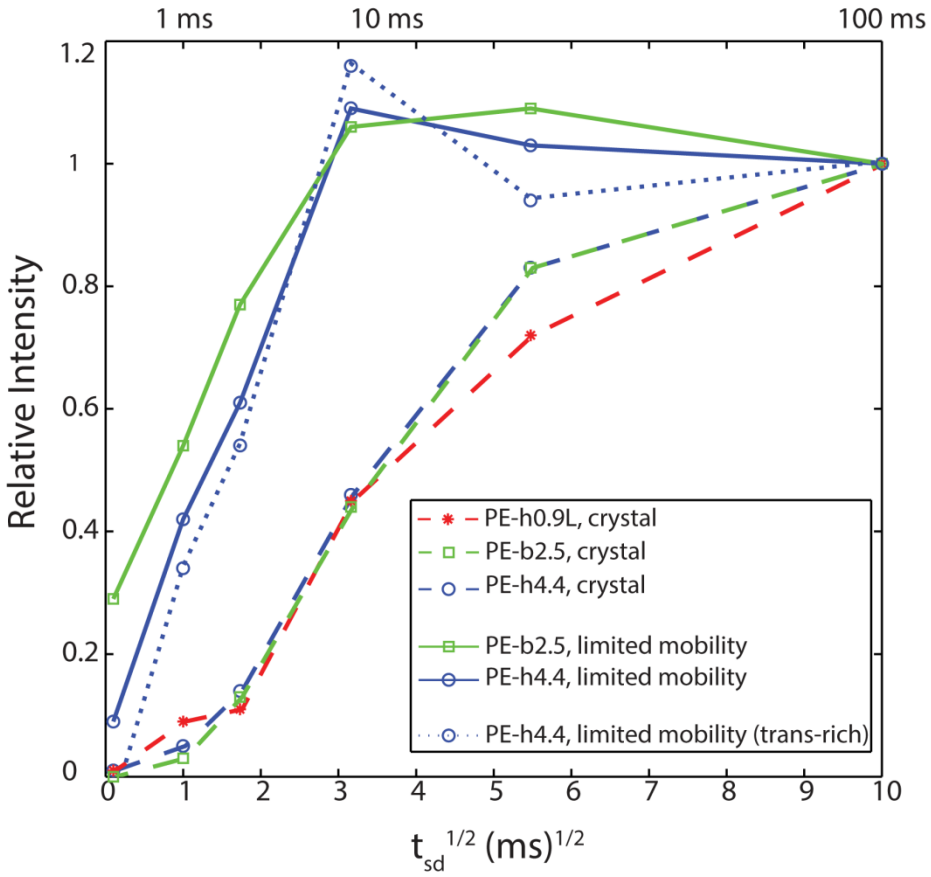


**Figure S.1.** Alternate presentation of the changing intensities of the peaks selected in the spectra shown in Figure 5.5.